Limited effect of the confluence angle and tributary gradient on Alpine confluence morphodynamics under intense sediment loads

Authors:

Théo St. Pierre Ostrander[1] – Corresponding Author

theo.st-pierre-ostrander@uibk.ac.at

Thomé Kraus[2]

Thome.Kraus@student.uibk.ac.at

Bruno Mazzorana[3]

bruno.mazzorana@uach.cl

Johannes Holzner[4]

Johannes.Holzner@provinz.bz.it

Andrea Andreoli[5]

Andrea.Andreoli@unibz.it

Francesco Comiti[6]

Francesco.Comiti@unibz.it

Bernhard Gems[7]

bernhard.gems@uibk.ac.at

[1, 2, 7] University of Innsbruck, Unit of Hydraulic Engineering, Technikerstraße 13a, 6020, Innsbruck, Austria

[3] Universidad Austral de Chile, Faculty of Sciences, Instituto de Ciencias de la Tierra, Edificio Emilio Pugín, Avenida Eduardo Morales Miranda, Campus Isla Teja, Valdivia, Chile

[4, 5, 6] Free University of Bozen-Bolzano, Faculty of Agricultural, Environmental and Food Sciences, Universitätsplatz 5 - piazza Università, 5, 39100, Bozen-Bolzano, Italy

Abstract

Confluences are dynamic morphological nodes in all river networks. In mountain regions, they are influenced by hydraulic and sedimentary processes occurring in steep channels during extreme events in small watersheds. Sediment transport in the tributary channel and aggradation in the confluence can be massive, potentially causing overbank flooding and sedimentation into adjacent settlement areas. Previous works dealing with confluences have been mainly focused on lowland regions, or if focused on mountain areas, the sediment concentrations and channel gradients were largely under-representative of mountain river conditions. The presented work contributes to filling this research gap with 45 experiments using a large-scale physical model. Geometric model parameters, applied grain size distribution, and the considered discharges represent the conditions at 135 confluences in South Tyrol (Italy) and Tyrol (Austria).

The experimental program allowed for a comprehensive analysis of the effects of (i) the confluence angle, (ii) the tributary gradient, (iii) the channel discharges, and (iv) the tributary sediment concentration. Results indicate, in contrast to most research dealing with confluences, that in the presence of intense tributary sediment supply and a small tributary to main channel discharge ratio (0.1), the confluence angle does not have a decisive effect on confluence morphology. Adjustments to the tributary channel gradient yielded the same results. A reoccurring range of depositional geomorphic units was observed where a deposition cone transitioned to a bank-attached bar. The confluence morphology and tributary channel gradient rapidly adjusted, tending towards an equilibrium state to accommodate both water discharges and the sediment load from the tributary. Statistical analyses demonstrated that confluence morphology was controlled by the combined channel discharge and the depositional or erosional extents by the sediment concentration. Applying the conclusions drawn from lowland confluence dynamics could misrepresent depositional and erosional patterns and the related flood hazard at mountain river confluences.

Keywords: Confluence Morphology; Fluvial Hazard; Steep Tributary; Bedload; Physical Scale Model; Mountain Rivers

1 Introduction

River confluences are important features of all river systems and are sites of significant hydraulic and morphological change (Benda et al., 2004). They are characterized by converging flow paths that produce complex 3-dimensional hydraulics that influence the local morphology, and fluvial dynamics (Best, 1987; 1988; Rhoads & Kenworthy, 1995; Benda et al., 2004; Boyer et al., 2006; Ferguson & Hoey, 2008; Guillén-Ludeña et al., 2015; Guillén-Ludeña et al., 2017). In developed areas, confluences form critical junctions as the hydraulic geometries and sediment loads from each channel must be accommodated to avoid overbank flooding and sedimentation (Gems et al., 2014; Liu et al., 2015; Kammerlander et al., 2016; Sturm et al., 2018). The importance of these junctions has garnered much research interest, which has illuminated many characteristics of the hydro-morphodynamic interactions, and the major controls on the flow structure occurring at lowland river confluences (Mosley, 1976; Best, 1987; 1988; Biron et al., 1993; Rhoads & Kenworthy, 1995; Bradbrook et al., 1998; De Serres et al., 1999; Benda et al., 2004; Boyer et al., 2006; Wang et al., 2007; Liu et al., 2015). Best (1987; 1988) built upon the seminal work of Mosley (1976) in his identification of hydraulic and morphologic zones occurring at confluences. The typically occurring hydraulic zones are: flow separation, flow stagnation, flow deflection, maximum velocity, shear layers, and the recovery zone. These zones influence sediment transport pathways through the confluence and the resulting morphological elements of confluences: avalanche faces at the mouth of each confluent channel, a deep central scour hole, and a bar in the separation zone. Best (1988) concluded that the controlling variables as to the location, orientation, and size of these morphologic zones are the confluence angle and the discharge ratio $Q_r = Q_t/Q_m$ which is the ratio of the tributary (Q_t) and the main channel (Q_m) discharges. For lowland confluences increasing the discharge ratio or the confluence angle leads to a greater mutual deflection of flows and a bigger separation zone, which is the largest sink for tributary-transported sediment (Best, 1987, 1988). Flow deflection influences the shear layers generated between the two convergent flows, along which powerful vortices are generated which are responsible for increased bed shear stresses in the junction (Mosley, 1976; Best, 1987; Penna et al., 2018; De Serres et al., 1999). Contrarily, decreasing the confluence angle results in a greater mixing of flows, a smaller separation zone, and declined levels of turbulence in the confluence (Best, 1988; Penna et al., 2018). However, mountain channels are steeper than lowland channels with higher velocities and supercritical flows that amplify event intensity (Rudolf-

Miklau et al., 2013) and can result in rapid channel adjustments (Wohl, 2010). This is apparent when comparing, for example, the Froude numbers from Best (1988) (0.1-1) and Biron et al. (1996) (0.1-0.24), and the tributary velocities (0.45 m s^{-1}-0.57 m s^{-1}) from Roy and Bergeron (1990) with the Froude numbers and velocities from the presented work (Table 1) and steep channels in the study region (e.g., Hübl et al., 2005).

Table 1 Experimental discharges for the main (Q_m) and tributary (Q_t) channels with corresponding hydraulic attributes showing flow depth (h), Froude (Fr), and velocity (v) upstream (u) and downstream (d) of the confluence and in the tributary channel (t), for all confluence angles (CA) and tributary gradients (trib.), values are based on undisturbed, initial conditions in the channel.

	Q_m [l s^{-1}]	Q_t [l s^{-1}]	Q_{tot} [l s^{-1}]	h_u [m]	h_t [m]	h_d [m]	Fr_u [-]	Fr_t [-]	Fr_d [-]	v_u [m s^{-1}]	v_t [m s^{-1}]	v_d [m s^{-1}]
CA 90° Trib. 10% [EXP 1-15]	15	1.5	16.5	0.04	0.01	0.03	0.58	2.04	0.77	0.35	0.68	0.44
	45	4.5	49.5	0.08	0.02	0.06	0.53	2.39	0.98	0.47	1.08	0.75
	75	7.5	82.5	0.11	0.03	0.08	0.59	2.79	1.00	0.61	1.43	0.89
	105	10.5	115.5	0.14	0.04	0.10	0.62	2.63	1.01	0.73	1.52	1.01
	135	13.5	148.5	0.17	0.04	0.12	0.66	2.87	1.06	0.84	1.76	1.16
CA 90° Trib. 5% [EXP 16-30]	15	1.5	16.5	0.05	0.01	0.04	0.46	1.55	0.69	0.31	0.57	0.42
	45	4.5	49.5	0.09	0.03	0.07	0.50	1.79	0.80	0.47	0.90	0.71
	75	7.5	82.5	0.12	0.04	0.09	0.51	1.84	1.02	0.56	1.08	0.93
	105	10.5	115.5	0.15	0.04	0.11	0.52	1.82	1.04	0.63	1.19	1.04
	135	13.5	148.5	0.18	0.05	0.13	0.52	1.90	0.97	0.69	1.34	1.08
CA 45° Trib. 10% [EXP 31-45]	15	1.5	16.5	0.04	0.01	0.04	0.56	1.79	0.69	0.35	0.60	0.42
	45	4.5	49.5	0.08	0.02	0.07	0.68	2.24	0.71	0.58	1.04	0.70
	75	7.5	82.5	0.11	0.03	0.09	0.61	2.54	0.96	0.64	1.34	0.89
	105	10.5	115.5	0.14	0.04	0.11	0.60	2.52	0.90	0.70	1.48	0.94
	135	13.5	148.5	0.16	0.04	0.13	0.61	2.77	0.95	0.77	1.72	1.07

Confluences in mountain regions have not received the same attention as those in lowland areas, which is surprising given the hazard potential associated with large volumes of coarse sediment entering these critical junctions (Aulitzky, 1989). Differentiation between mountain and lowland confluences can be described by (i) supercritical or transitioning flow conditions in the tributary channel, (ii) bed surface armoring due to the size heterogeneity of the tributary sediment load or non-erodible conditions in the tributary channel as a result of hazard protection measures, (iii) high sediment concentrations during flooding events and (iv) highly variable discharges and sediment transport rates (Aulitzky, 1980; 1989; Meunier, 1991; Roca

et al., 2009; Guillén-Ludeña et al., 2017). Topographic confinement can amplify confluence effects, whereas in lowland regions with wide valley floors and broad terraces, deposition cones or fans can be isolated from the main channel (Benda et al., 2004). A sudden introduction of sediment from steep tributaries can trigger numerous types of morphological changes (Benda et al., 2004), as tributaries of confined channel confluences can be particularly impactful (Rice, 1998).

Detailed records of flash flooding associated with intense sediment transport in Tyrol (Austria) show that these events are a persistent hazard (Embleton-Hamann, 1997; Rom et al., 2023). In the Alps, hazardous events can impact high-population-density valleys. Increased or shifting flooding patterns (Blöschl et al., 2017; Löschner et al., 2017; Blöschl et al., 2020; Hanus et al., 2021) and enhanced sediment availability (Knight & Harrison, 2009; Stoffel et al., 2012; Gems et al., 2020) as a consequence of climate change (Keiler et al., 2010) not only threatens new infrastructure but challenges previously installed mitigation measures. Ancey (2020a) discusses the complications, and assumptions associated with the multitude of approaches used to predict bedload transport and the resulting bedforms, and how rivers are systems punctuated by intense moments of bedload transport resulting in rapid changes in bed morphology over short time intervals (Ancey, 2020b). Relevant hazard events are typically triggered by localized short-duration-high intensity convective storms occurring in small watersheds, which do not significantly affect main channel discharge and bedload transport (Gems et al., 2014; Hübl & Moser, 2006; Prenner et al., 2019; Stoffel, 2010). The narrow, steep tributary provides the sediment load to the main channel, which supplies the dominant flow discharge (Miller, 1958; Guillén-Ludeña et al., 2017).

Most of the work that has been done on mountain river confluences has been focused on conditions that do not typically generate hazardous events, mainly under-representations of gradients and sediment concentrations (Roca et al., 2009; Leite Ribeiro et al., 2012a; Leite Ribeiro et al., 2012b; Guillén-Ludeña et al., 2015; Guillén-Ludeña et al., 2017). Complicating the conclusions drawn regarding confluence morphodynamics, St. Pierre Ostrander et al. (2023) established, from a set of 15 experiments, that confluences of mountain rivers are influenced by factors other than the confluence angle and the discharge ratio. They held the confluence angle and discharge ratio constant, only adjusting discharges and tributary sediment concentration. They observed a range of morphologies with specific geomorphic units: a deposition cone, a transitional morphology, a bank-attached bar, and a scour hole. They used unit stream

power to predict and associate confluence zone morphology with hydraulic conditions. However, they were limited in their conclusions and recommended further experiments considering additional geometries as their experimental program was not sufficiently comprehensive, restricting the reach of their findings. The channel geometry was unchanged throughout the experimental program, and morphological assessment lacked statistical evaluation and grain size analysis. This paper builds upon these experimental results with an additional 30 experiments considering geometric modifications. In addition to investigating the effects of the channel discharge and sediment concentration, adjustments to the confluence angle and the tributary gradient provide a more comprehensive data analysis of fluvial hazard processes and the resulting morphologies of mountain river confluences. Evaluating morphological patterns and extents was done qualitatively with DEMs of Difference (DoD) created from laser scans, quantitatively from the extents of geomorphic units, depositional and erosional values, and volumetric grain samples, and statistically. Statistical analyses determined which of the introduced controlling factors significantly impacted the response variables that define the morphodynamic development of mountain river confluences. Results from the 45 experiments tested the following hypotheses:

1. Adjustments to the confluence angle and the tributary gradient do not significantly impact confluence morphology and the development of specific geomorphic units (hypothesis 1).
2. Of the introduced controlling factors, the sediment concentration and channel discharge exert the most control over depositional and erosional patterns (hypothesis 2).

The formulation of the two hypotheses was based on the results of St. Pierre Ostrander et al. (2023) where it was established that in addition to the confluence angle and discharge ratio, there were additional factors influencing the morphological development of the confluence, and from a review of literature dealing with rivers in response to intense hydrological events. Specifically, a channel will adjust its geometric characteristics and gradient in a way that maximizes sediment transport capacity (Lane, 1955; White et al., 1982).

2 Model and Methods

2.1 Experimental program

The physical scale model (Fig. 1) was constructed to represent a typical confluence in the regions of South Tyrol (Italy) and Tyrol (Austria). The experimental setup served as a generic configuration to reproduce the main hydrodynamic and sedimentary processes occurring at mountain river confluences while gaining insights into the dominant control variables. Experimental modeling uses and builds upon the configuration, calibration, and experiments (1-15) carried out by St. Pierre Ostrander et al. (2023), but considers an additional case for the tributary gradient as well as for the confluence angle. Model dimensions, discharges, and the grain size distribution of the quartz sand input material and the main channel bed were based on an analysis of 135 confluences and 65 volume (subsurface) and line (surface) sediment samples in the study region (St. Pierre Ostrander et al., 2023). The sediment mix was scaled by a factor of 30 to transfer natural grain size dimensions to model conditions. The main channel had a mobile bed, allowing for 0.2 m of erosion while the tributary channel had a fixed bed. Tributary bed roughness was created using an adhesive to apply a layer of quartz sand to the bed. Channel roughness was established through hydraulic manuals (Chow, 1959) and previous calibration work (St. Pierre Ostrander et al., 2023). Quartz sand is widely used in flume experiments dealing with gravel bed rivers (e.g., Williams, 1970; Gems et al., 2014), as the grain density (ρ_s=2650 kg m^{-3}) supports Froude model similitude (Young & Warburton, 1996). A grain size distribution curve and the gradation coefficient (σ) of both the mobile bed and the input material are included in Fig. 1. The physical model was adjustable, except for the width of the tributary (0.2 m) and the lengths of the channels (5.0 m and 9.0 m for the tributary and main channel, respectively). Discharge to each channel was supplied by separate pumps controlled by electronic flow measurement devices. The discharge ratio was fixed at 0.1 for all experiments. The tributary sediment discharge was always proportional to the clear water discharge; an increase in tributary discharge meant an increase in both clear water and sediment discharges. The main channel flow was exclusively clear water and fully rough turbulent to replicate typical events that produce massive aggradation at mountain river confluences (Hübl & Moser, 2006; Stoffel, 2010; Gems et al., 2014; Prenner et al., 2019). Scaling was done according to Froude similarity; transferring model dimensions to nature allows a scale factor range of 20-40. The scale is

176 determined by the width of the tributary at the confluence relative to the width of the tributary in the physical
177 model and is referred to as the specific scale (St. Pierre Ostrander et al., 2023).

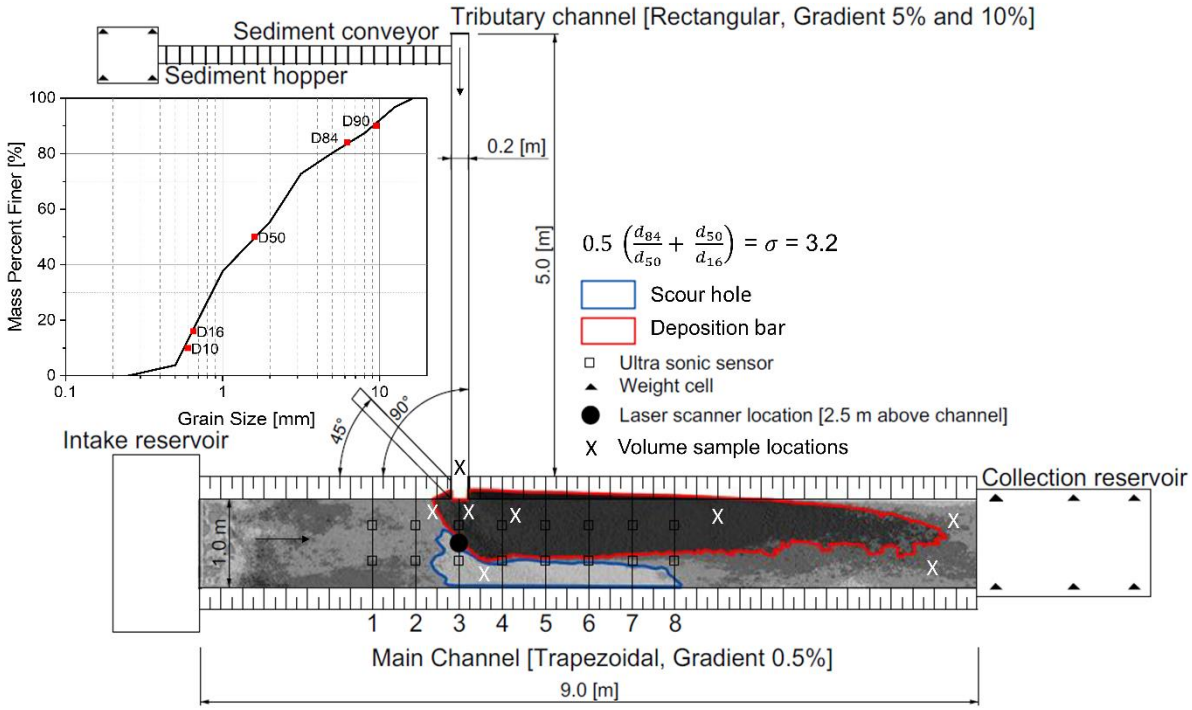

178

179 **Figure 1** Overview of the physical model showing the location of measurement devices, volume sample
180 locations, the gradation coefficient (σ), the grain size distribution of the sediment supplied to the tributary
181 channel and the mobile bed in the main channel, and an example of the scour hole and the deposition bar.

182

183 Experiments (Table 2) allowed for the same 5 steady-state discharge combinations to be tested with
184 different tributary gradients, confluence angles, and sediment concentrations, which were based on the bulk
185 density of the input material. The 5 discharges correspond to flooding conditions in the study region,
186 including an extreme event. Steady-state discharges were used so a specific discharge could be linked with
187 a geomorphic unit, to limit uncertainty in associating morphologies with the introduced controlling factors,
188 which is consistent with other researchers dealing with steep channel confluences, (Roca et al., 2009; Leite
189 Ribeiro et al., 2012), and to make the morphological development comparable to research dealing with
190 lowland confluences, which largely assume steady-state conditions (e.g., Mosley, 1976; Best, 1988). The
191 morphological development of the confluence zone for each geometric setup was evaluated by creating
192 DEMs of Difference (DoD) (*ESRI ArcGIS Desktop, Release 10.8.2*) from laser scans (*Faro Focus 3D,*

193 *Trimble X7*) taken before and after an experiment. Each laser scan contained 125 million points with a point
194 density of 0.004 m at a distance of 10 m. The average error between the position of the scanner and the
195 targets used for referencing the scans was less than 0.004 m. The initial bathymetry was the reference,
196 which was established by running a low discharge of 15 l s^{-1} in the main channel for 5 hours to create a
197 more natural river bed, while the post-run bathymetry was the comparison (St. Pierre Ostrander et al., 2023).
198 Morphological evaluation was done by assessing specific zones and overall changes occurring in the
199 channel. The deposition bar and scour hole were delineated by deposition or erosion above or below 0.01
200 m (Fig. 1). Main channel deposition and erosion areas and volumes reflect morphological change occurring
201 throughout the entire channel above or below the initial bathymetry.

202 Based on incident reports supplied by the Austrian Service for Torrent and Avalanche Control and event
203 documentation (e.g. Hübl et al., 2012), the scaled (30), according to Froude similarity, experiment duration
204 was 20 minutes and started when sediment entered the tributary channel. The only alterations between the
205 experimental groups were changing the tributary gradient and the confluence angle. Experiments 1-15 had
206 a 10% tributary gradient, a 90° confluence angle, and a main channel gradient of 0.5%. Experiments 16-30
207 had the same geometric configuration except with a 5% tributary gradient. Experiments 31-45 had a 10%
208 tributary gradient and a 45° confluence angle; the main channel gradient remained unchanged. The
209 respective dimensions were chosen as they are the most representative of the study region (St. Pierre
210 Ostrander et al., 2023). DEMs of Difference were created from the DoDs of experiments with identical input
211 conditions, i.e., discharge and sediment supply rate, allowing for a visual assessment of morphological
212 differences based on geometric changes alone. For example, experiments 1 and 16 had equal discharges
213 and sediment concentrations; the only change was the tributary gradient, and experiments 1 and 31 had
214 the same discharges, sediment concentrations, and gradients, but the confluence angle was changed. The
215 10% gradient tributary with a 90° confluence angle was used as the reference as both geometric
216 configurations are comparable, and changes from the gradient and confluence angle could be accurately
217 assessed.

Table 2 Experiment target and actual discharges and sediment concentration, and tributary sediment supply rate, Q denotes discharge while m or t subscripts refer to the main channel and the tributary channel, respectively. The main channel gradient was 0.5% for all experiments. Experiment 30 could not be completed as the deposition in the tributary caused overtopping of the channel.

	EXP [-]	Q_m Target [l s^{-1}]	Q_m Actual [l s^{-1}]	Q_t Target [l s^{-1}]	Q_t Actual [l s^{-1}]	Sed. conc. Target [%]	Sed. conc. Actual [%]	Sed. supply rate [kg min^{-1}]
10% Tributary Gradient 90° Confluence Angle	1	15.0	15.3	1.5	1.5	5.0	*	7.6
	2	45.0	45.6	4.5	4.3	5.0	*	22.9
	3	75.0	75.5	7.5	7.4	5.0	5.7	43.5
	4	105.0	104.5	10.5	10.6	5.0	4.9	53.4
	5	135.0	135.4	13.5	13.4	5.0	5.2	68.7
	6	15.0	15.1	1.5	1.5	7.5	7.6	11.4
	7	45.0	46.1	4.5	4.4	7.5	7.5	34.3
	8	75.0	75.3	7.5	7.5	7.5	7.3	57.2
	9	105.0	105.1	10.5	10.5	7.5	7.6	80.1
	10	135.0	134.7	13.5	13.4	7.5	7.5	103.0
	11	15.0	14.8	1.5	1.5	10.0	*	15.3
	12	45.0	44.9	4.5	4.6	10.0	10.1	45.8
	13	75.0	76.1	7.5	7.6	10.0	10.3	76.3
	14	105.0	105.7	10.5	10.4	10.0	10.4	106.8
	15	135.0	135.4	13.5	13.6	10.0	*	137.3
5% Tributary Gradient 90° Confluence Angle	16	15.0	15.9	1.5	1.4	5.0	*	7.6
	17	45.0	46.0	4.5	4.5	5.0	5.1	22.9
	18	75.0	75.9	7.5	7.6	5.0	5.0	43.5
	19	105.0	104.4	10.5	10.4	5.0	5.1	53.4
	20	135.0	134.7	13.5	13.5	5.0	5.2	68.7
	21	15.0	15.5	1.5	1.4	7.5	*	11.4
	22	45.0	46.7	4.5	4.3	7.5	7.8	34.3
	23	75.0	74.9	7.5	7.5	7.5	7.5	57.2
	24	105.0	105.5	10.5	10.4	7.5	7.5	80.1
	25	135.0	134.6	13.5	13.4	7.5	7.9	103.0
	26	15.0	15.1	1.5	1.6	10.0	9.6	15.3
	27	45.0	43.5	4.5	4.4	10.0	10.2	45.8
	28	75.0	75.0	7.5	7.6	10.0	10.1	76.3
	29	105.0	105.9	10.5	10.5	10.0	10.1	106.8
	30	135.0	-	13.5	-	-	-	-
10% Tributary Gradient 45° Confluence Angle	31	15.0	14.6	1.5	1.6	5.0	*	7.6
	32	45.0	45.0	4.5	4.3	5.0	5.2	22.9
	33	75.0	75.8	7.5	7.7	5.0	4.9	43.5
	34	105.0	105.1	10.5	10.5	5.0	5.0	53.4
	35	135.0	134.9	13.5	13.5	5.0	5.0	68.7
	36	15.0	15.0	1.5	1.5	7.5	*	11.4
	37	45.0	45.6	4.5	4.5	7.5	7.6	34.3
	38	75.0	75.2	7.5	7.5	7.5	7.7	57.2
	39	105.0	106.1	10.5	10.5	7.5	7.6	80.1
	40	135.0	135.6	13.5	13.4	7.5	8.0	103.0
	41	15.0	14.8	1.5	1.4	10.0	10.4	15.3
	42	45.0	44.9	4.5	4.4	10.0	10.1	45.8
	43	75.0	75.5	7.5	7.6	10.0	9.9	76.3
	44	105.0	105.8	10.5	10.4	10.0	9.3	106.8
	45	135.0	135.0	13.5	13.5	10.0	*	137.3

*indicates that the sediment was delivered manually or with manual assistance as the dosing machine could not dose very low or high rates of sediment into the tributary channel

2.2 Statistical analysis

A statistical analysis of the various introduced controlling factors and their effects on the response variables (Table 3) was done using the software package *OriginPro (v.2023, OriginLab Corp.)* (Stevenson, 2011; Baranovskiy, 2019). The chosen response variables (Table 3), captured either depositional or erosional features and allowed for a nuanced investigation into the subtle morphological variations that were not able to be qualitatively assessed. The combined discharge was used as a factor since the morphological development of the confluence occurred downstream of the tributary. The confidence interval for all tests was 95%. A significant result occurred when the p-value, calculated from the test statistic of the applied test, was less than 0.05. A p-value less than 0.05 allowed for rejecting the null hypothesis, which was the factor that did not significantly impact the response variable. If rejected, further pairwise post hoc tests were conducted to determine the decisive factors influencing confluence morphology.

Table 3 Controlling factors and response variables that control and define confluence morphology.

Factor	Unit	Response Variable	Unit
Sediment concentration (5, 7.5, 10)	%	Main channel deposition area and volume	m^2, m^3
Combined discharge (16.5, 49.5, 82.5, 115.5, 148.5)	$l\ s^{-1}$	Main channel erosion area and volume	m^2, m^3
Confluence angle (90, 45)	°	Deposition bar area	m^2
Tributary gradient (10, 5)	%	Deposition bar length	m
		Deposition bar width	m
		Scour area	m^2
		Scour length	m
		Scour width	m
		Maximum depths scour and deposition	m

The sequence of operations in Fig. 2 shows the chosen tests, which allowed for planned comparisons (Ruxton & Beauchamp, 2008). The relevant data sets were examined to ensure that the correct statistical and pairwise post hoc tests were applied (Welch, 1947; Massey, 1951; Dunn, 1964; Maxwell & Delaney, 2004; Steinskog et al., 2007; Sawyer, 2009; McKnight et al., 2010; Moder, 2010; Witte & Witte, 2017;

Delacre et al., 2019). Determining which tests were applied for a specific factor was based on the sample coming from a population of a specific distribution, then verifying heterogeneity or homogeneity of variances. This established the following hypothesis and subsequent post hoc tests, if applicable. Not all the tests were used but were established in case of varying distributions and homogeneity or heterogeneity of variances. Data was grouped by aggregating individual observations for a specific controlling factor. For example, the deposition bar area in response to sediment concentration would have 3 groups, a mean area for each of the 3 tested sediment concentrations; for the confluence angle, the bar area can only have 2 mean values 1 from each angle, so there are only 2 groups.

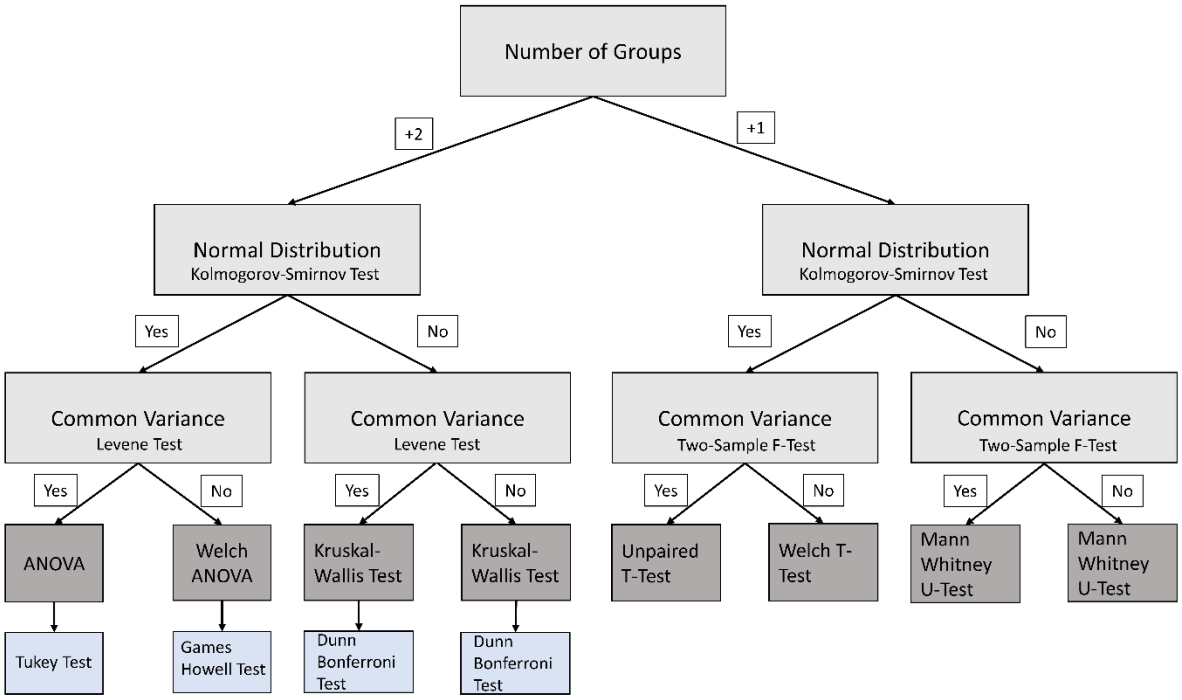

Figure 2 Workflow for assessing the impact of controlling factors with associated tests based on the number of groups, and the distributions and variances of the examined data sets.

2.3 Volumetric grain sampling

Volume samples were taken after each experiment with sample locations corresponding to confluence morphologic (Best, 1988) and hydraulic zones (Best, 1987) in the channel. In total 8 samples were taken

for each experiment. The sampled volume was 0.002 m^3 with an average sample mass of 3.3 kg which was taken by inserting a cylinder (0.16 m diameter and 0.1 m height) into the channel bed or depositional form. The sampled mass was within the guidelines of Bunte and Abt (2001) (Eq. 2):

$$\text{Mass}_{\text{sample}}\ (\text{kg}) = 0.1 * 10^{b} * \rho_s * D_{max}^{3} \qquad \text{(Equation 2)}$$

Where D_{max} is the maximum grain size (16 mm), ρ_s is grain density (2650 kg m^{-3}), b is the accuracy level, high (b=5), medium (b=4), low (b=3). A larger volume would not be suitable to accurately represent small areas of deposition or erosion as material outside of the area of interest would be additionally captured. The samples were dried after collection and before the sieving analysis. During sieving the material was separated into 10 fractions based on the mesh size of each sieve. The masses of each fraction were determined and plotted as grain size distribution curves. This grain size analysis provided insights into the hydraulic influence on the various zones.

3 Results

3.1 Development and evolution of confluence morphology

Table 4 associates the three depositional geomorphic units consistently observed for all channel configurations and sediment concentrations with unit stream power. Unit stream power calculations are based on initial conditions at a cross-section in the main and tributary channels. The geomorphic units were (i) the deposition cone (Fig. 3a, Appendix 1a to 9a), (ii) transitional morphology (Fig. 3b, Appendix 1b to 9b), and (iii) the attached-to-the-left-channel-wall separation zone bar (Fig. 3c, Appendix 1c-e to 9c-e). The scour hole, an erosional geomorphic unit (Fig. 3), was apparent in all experiments (Appendix 1-9) on the right bank opposite the tributary. The deposition cone was characterized by deposition upstream of the confluence in the main channel, a compact longitudinal extent, and steep gradients in upstream and downstream directions (Fig 3d). Cone formation resulted from insufficient transport capacity of the main channel flow and a sustained and abundant sediment supply from the tributary channel. Deposition cones formed for all configurations and sediment concentrations when the discharge was 15 l s^{-1} and 1.5 l s^{-1} in

the main and tributary channels, respectively. The transitional morphology is derived from increased discharge and subsequent unit stream power where experimental discharges of 45 l s^{-1} in the main and 4.5 l s^{-1} in the tributary had nearly forced the bar over to the left bank, but morphological aspects of the deposition cone remained. The transitional morphology partially occupies the separation zone, which is shown in Fig. 3e where the longitudinal profile is a hybrid between the cone and bar. Discharges and related unit stream power above 45 l s^{-1} in the main and 4.5 l s^{-1} in the tributary allowed for the development of an attached-to-the-left-channel-wall separation zone bar. The bar had the greatest longitudinal extent (Fig 3f) and the largest storage capacity for tributary-transported sediment. Once the separation zone bar was fully developed, the hydraulic separation zone was filled with deposited sediment and flanked by the maximum velocity zone on the right, which has been observed at lowland confluences with subcritical flows and larger discharge ratios (Best, 1988; Biron et al., 1993; De Serres et al., 1999).

Table 4 Geomorphic units and unit stream power (ω) values. Unit stream power was calculated for the main, tributary, and combined channel discharges. The subscripts *m* and *t* denote main and tributary channel conditions, respectively while *tot* represents the unit stream power from the combined channel discharge.

EXP [-]	ω_m	ω_t [W m^{-2}]	ω_{tot}	EXP [-]	ω_m	ω_t [W m^{-2}]	ω_{tot}	EXP [-]	ω_m	ω_t [W m^{-2}]	ω_{tot}	Geomorphic Unit [-]
1	0.8	7.5	0.8	**16**	0.8	3.4	0.9	**31**	0.7	7.8	0.8	Deposition cone
2	2.2	21.3	2.5	**17**	2.3	11	2.5	**32**	2.2	21.2	2.4	Transitional
3	3.7	36.4	4.1	**18**	3.7	18.6	4.1	**33**	3.7	37.6	4.1	Attached-to-channel bar
4	5.1	51.9	5.7	**19**	5.1	25.6	5.6	**34**	5.2	51.3	5.7	Attached-to-channel bar
5	6.6	65.9	7.3	**20**	6.6	33.2	7.3	**35**	6.7	66.2	7.3	Attached-to-channel bar
6	0.7	7.2	0.8	**21**	0.8	3.5	0.8	**36**	0.7	7.5	0.8	Deposition cone
7	2.3	21.7	2.5	**22**	2.3	10.6	2.5	**37**	2.2	21.8	2.5	Transitional
8	3.7	36.6	4.1	**23**	3.7	18.3	4.0	**38**	3.7	36.8	4.1	Attached-to-channel bar
9	5.2	51.4	5.7	**24**	5.2	25.6	5.7	**39**	5.2	51.4	5.7	Attached-to-channel bar
10	6.6	65.8	7.3	**25**	6.6	32.9	7.3	**40**	6.7	65.7	7.3	Attached-to-channel bar
11	0.7	7.4	0.8	**26**	0.7	3.8	0.8	**41**	0.7	7.0	0.8	Deposition cone
12	2.2	22.4	2.4	**27**	2.1	10.9	2.4	**42**	2.2	21.4	2.4	Transitional
13	3.7	37.5	4.1	**28**	3.7	18.7	4.1	**43**	3.7	37.4	4.1	Attached-to-channel bar
14	5.2	51.2	5.7	**29**	5.2	25.7	5.7	**44**	5.2	51.1	5.7	Attached-to-channel bar
15	6.6	66.6	7.3	**30**	-	-	-	**45**	6.6	66.1	7.3	Attached-to-channel bar

The scour hole was created hydraulically by the extent of the separation zone forcing the confluent streams to a smaller area, and physically by channel constriction resulting from depositional patterns reducing the

area in which the confluent flows may travel (Guillén-Ludeña et al., 2015; St. Pierre Ostrander et al., 2023), thereby increasing flow velocities (Rhoads and Kenworthy, 1995) and transport capacities. Additionally, the absence of avalanche faces inhibits the development of lee-side flow separation cells (Roy & Bergeron, 1990), which segregates sediment around the confluence instead of through it. Field observation of a gravel-bed confluence showed that tracked particles from both channels converge towards the scour hole with no noticeable segregation (Roy & Bergeron,1990). As the hydraulic separation zone filled with sediment, the spatial extent of the scour hole increased. The system tended towards an equilibrium state where sediment was transported through the scour hole, as this was the only available pathway through the confluence. The size and depth of the scour hole were greatest at lower sediment concentrations, given the same discharge. There was less sediment to be transported and potentially deposited in the scour hole, and the transport capacity of the main channel was not yet exhausted.

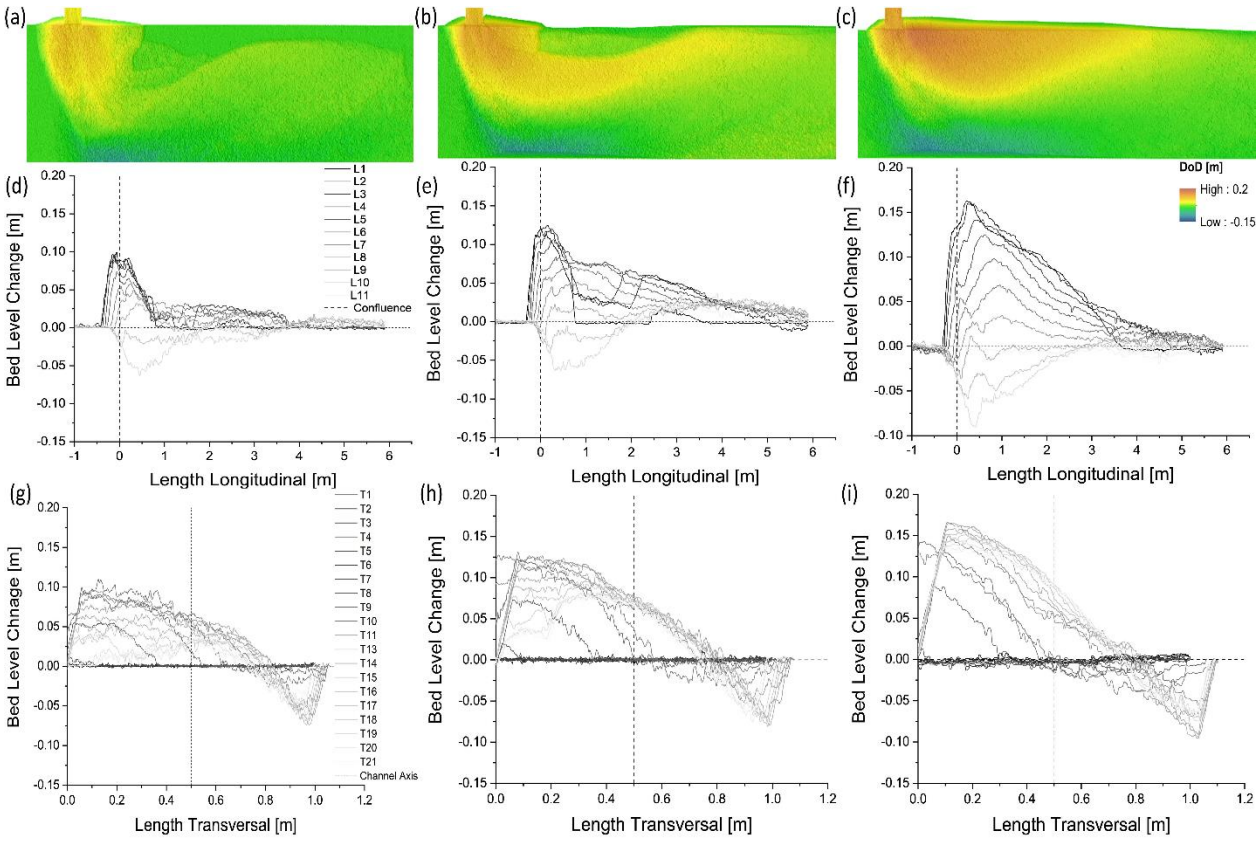

Figure 3 Observed geomorphic units, the deposition cone (a) shown with longitudinal (d) and transversal plots (g), the transitional morphology (b) shown with longitudinal (e) and transversal plots (h), and the attached-to-channel-wall separation zone bar (c) shown with longitudinal (f) and transversal plots (i) with

the scour hole on the right, opposite the tributary. Longitudinal profiles were spaced every 0.1 m and spanned 7 m, starting 1 m upstream of the confluence, transversal profiles were spaced every 0.1 m, starting 1 m upstream of the confluence, and spanned 2 m, focusing on the confluence zone.

3.2 Effects of the tributary gradient

Figure 4 shows the DoDs from the minimum (Fig 4a, d, g), median (Fig 4b, e, h), and maximum (Fig 4c, f) experimental discharge combinations which were produced by subtracting the DoDs from experiments 16-30, with a 5% tributary gradient from experiments 1-15, with a 10% tributary gradient. The same general morphological patterns consistently occurred regardless of the imposed geometric change. Intense bedload transport in the tributary provided an abundance of sediment to the confluence. A smaller tributary gradient of 5% (EXP 16-30) led to reduced velocity and subsequent transport capacity which did not greatly impact the morphological development of the confluence, relative to the depositional forms observed when the gradient was 10% (EXP 1-15). This trend could be associated with the unit stream power of the main channel since the same patterns were observed for all sediment concentrations. As described by Guillén-Ludeña et al. (2017), the main channel supplies the dominant flow at mountain river confluences, if the flow is unchanged then similar development occurs. Main channel unit stream power was consistent for all comparable experiments, the tributary unit stream power was approximately halved when the channel gradient was reduced to 5% (EXP 16-30) (Table 4).

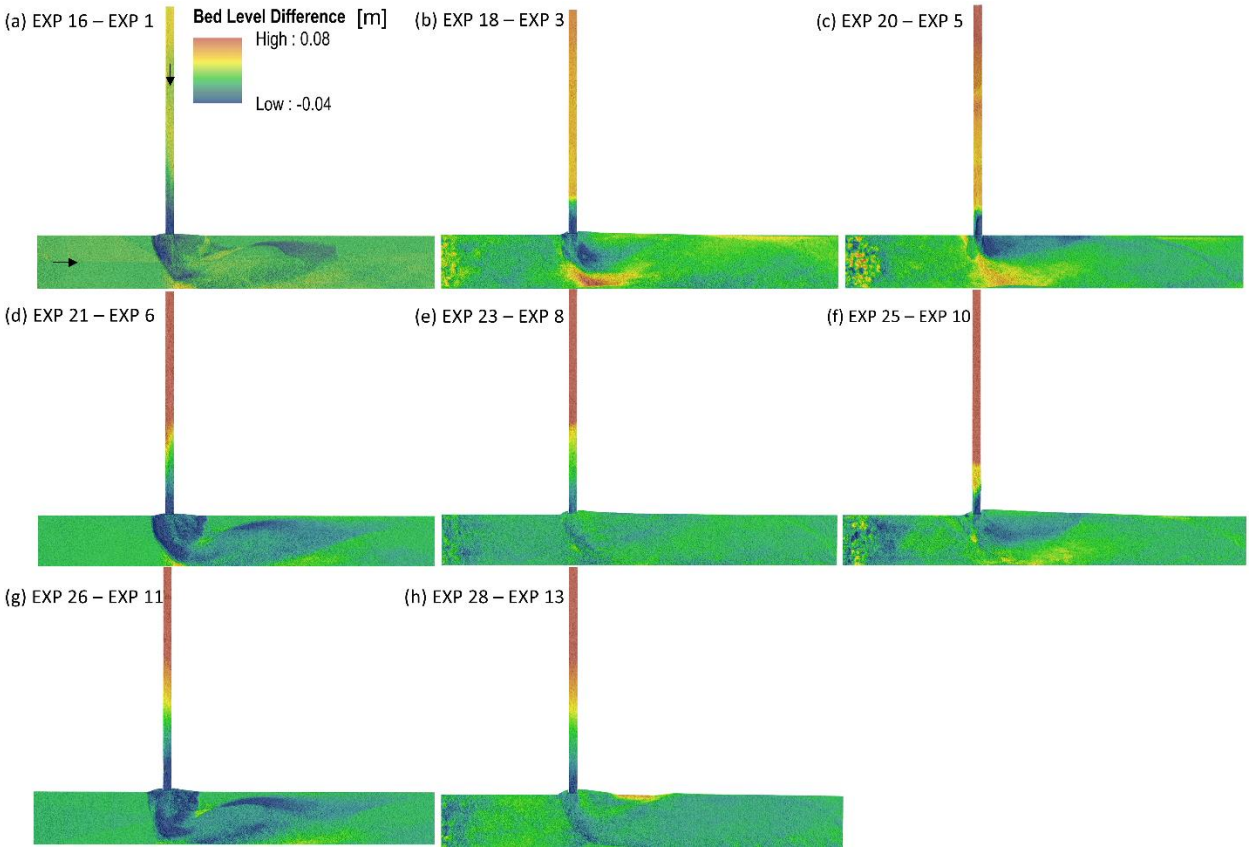

338

339 **Figure 4** DoDs showing the morphological differences between the minimum (a ,d, g), median (b, e, h), and
340 maximum (c, f) experimental discharges which were created by subtracting the DoDs from experiments with
341 a 5% tributary gradient (EXP 16-30) from the DoDs with a 10% tributary gradient (EXP 1-15).

342

343 Figure 5 shows the depositional and erosional characteristics of experiments 1-15 (10% tributary gradient,
344 90° confluence angle) and 16-30 (5% tributary, 90° confluence angle) excluding the tributary channel. A
345 visual inspection of Fig. 5 does not show a clear trend in differences in depositional or erosional
346 characteristics between gradients. What trend could be inferred is most apparent when comparing the first
347 5 experiments for each geometry group (EXP 1-5 and EXP 16-20). Depositional patterns (Fig. 5a, 5c, and
348 5e) were greater for experiments 16-20 than for experiments 1-5, while erosional patterns were greater for
349 experiments 1-5 than for 16-20 (Fig. 5b, 5d, and 5f). Reducing the tributary channel gradient reduced the
350 velocity of the tributary flow (Table 1), limiting its contribution to main channel erosion. When the tributary
351 gradient was 10% (EXP 1-15), there was greater penetration of the tributary flow into the main channel and

a local increase in transport capacity, creating a larger and deeper scour hole and enhanced conveyance of sediment through the confluence.

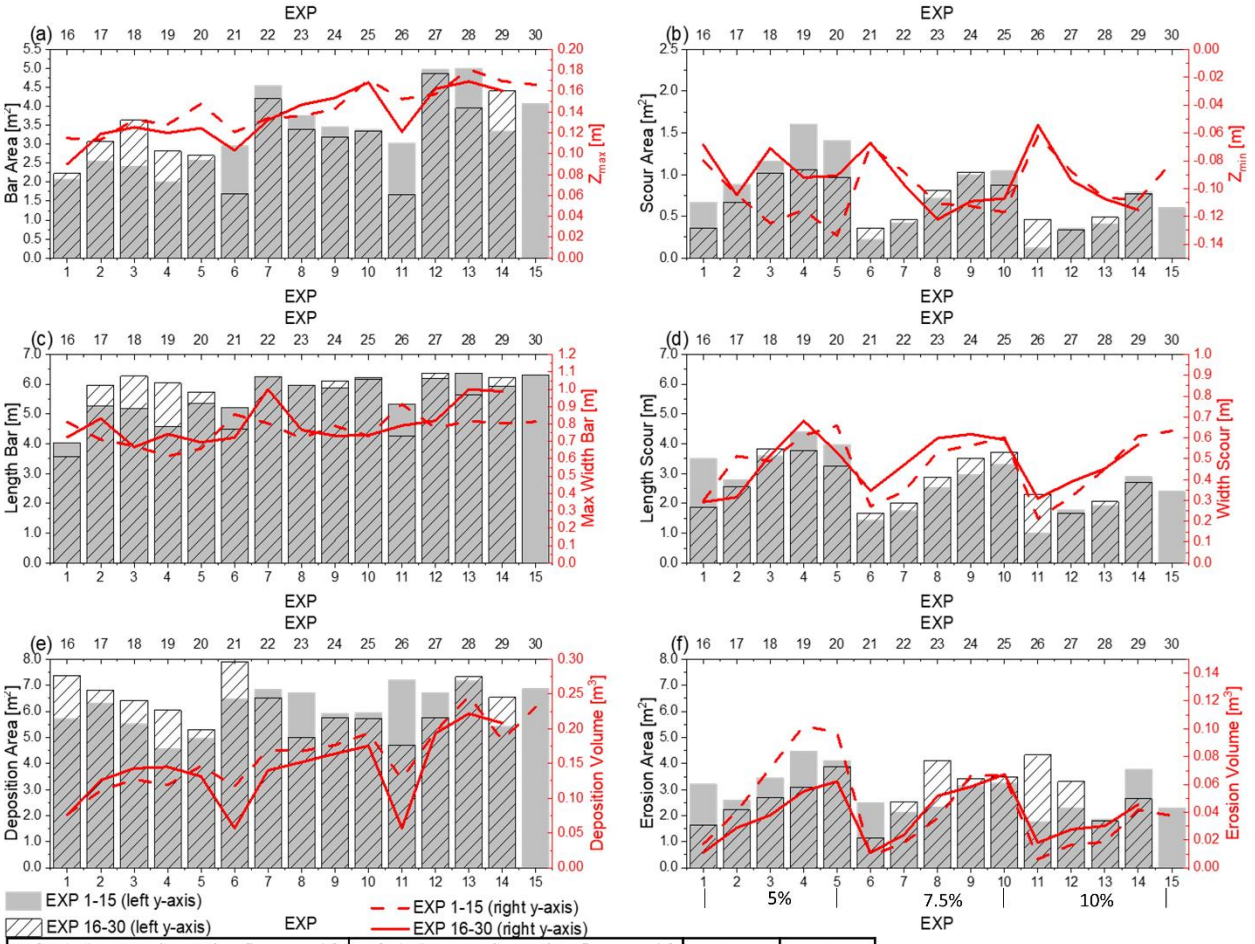

EXP [10% tributary gradient, 90° confluence angle]	EXP [5% tributary gradient, 90° Confluence angle]	Q_m	Q_t
[-]	[-]	[l s^{-1}]	[l s^{-1}]
1, 6, 11	16, 21, 26	15	1.5
2, 7, 12	17, 22, 27	45	4.5
3, 8, 13	18, 23, 28	75	7.5
4, 9, 14	19, 24, 29	105	10.5
5, 10, 15	20, 25, 30	135	13.5

Figure 5 A comparison of morphological attributes across experiments with a 5% (EXP 16-30) and 10% tributary gradient (EXP 1-15), sediment concentration groups are shown in panel f. Deposition bar and scour areas (a, b) are delineated by deposition or erosion above or below 0.01 m, respectively. The width and length values represent the maximum measured width or length (c, d), while the main channel deposition and erosion areas (e, f) represent all deposition and erosion in the main channel.

Figure 6 shows the gradients and volumes of the deposited sediment in the tributary channel at the end of experiments 1-30. The depositional gradient was determined through a linear regression of the DoD surface profile of the tributary channel. Adjustments to the tributary gradient changed the depositional mechanisms in the tributary channel, characterized by either an increase or decrease in the gradient of the deposited material in the tributary channel, relative to the initial gradient. When the initial gradient was 10% (EXP 1-15), the transport capacity of the main channel was the limiting factor for sediment moving through the confluence. This led to a regressive aggradation of sediment, starting at the junction, which decreased the gradient of the tributary channel. Conversely, when the initial tributary channel gradient was 5% (EXP 16-30), the resulting decrease in velocity saturated the transport capacity of the tributary channel. Consequently, the depositional patterns switched, and intense progressive deposition occurred starting at the upstream boundary of the tributary channel which increased the gradient of the channel.

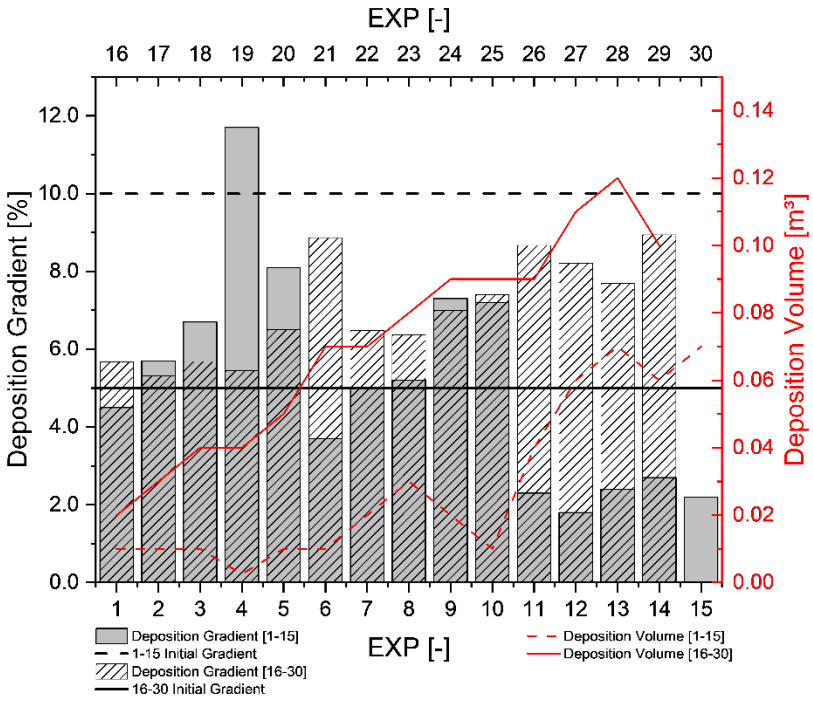

Figure 6 Gradients and volumes of deposited sediment in the tributary channel for experiments 1-15 with an initial 10% tributary gradient and experiments 16-30 with an initial 5% tributary gradient.

3.3 Effects of the confluence angle

Figure 7 shows the DoDs from the minimum (Fig 7a, d, g), median (Fig 7b, e, h), and maximum (Fig 7c, f, i) experimental discharge combinations which were created by subtracting the DoDs produced from experiments with a 45° confluence angle (EXP 31-45) from the DoDs with a 90° confluence angle (EXP 1-15). The tributary channels with a 45° confluence angle were extracted and referenced to the 90° tributary channels allowing for DoD comparisons. A visual inspection of confluence zone morphology does not reveal drastic changes between confluence angle experiments. Small regions of morphological change are apparent, mainly increased deposition downstream of the junction corner and a generally shallower scour hole when the confluence angle was 45°.

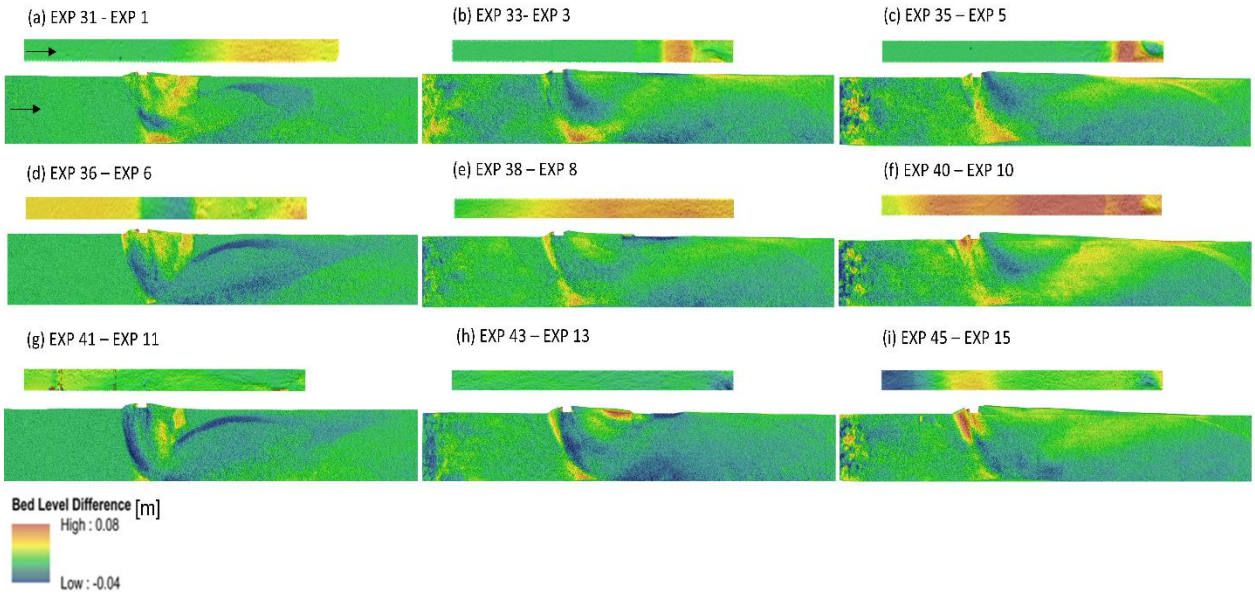

Figure 7 DoDs showing the morphological differences between the minimum (a, d, g), median (b, e, h), and maximum (c, f, i) experimental discharges which were created by subtracting the DoDs from experiments with a 45° confluence angle (EXP 31-45) from the DoDs with a 90° confluence angle (EXP 1-15).

Figure 8 shows subtle morphological differences with noticeable trends of scour characteristics, while depositional characteristics do not exhibit standout trends upon visual assessment. Both the area and length of the scour hole tended to be greater for experiments 31-45, with a 45° confluence angle (Fig. 8b and 8d).

However, the depth of scour and width of the scour was generally greater for experiments 1-15, with a 90° confluence angle. For both confluence angle experiment groups, a clear trend of increasing scour area, length of scour, and erosion area occurred within each sediment concentration group, increasing in response to discharge. Assessing the impact of confluence angle adjustments on depositional attributes required a statistical approach to reveal any nuanced relationships occurring within the channel.

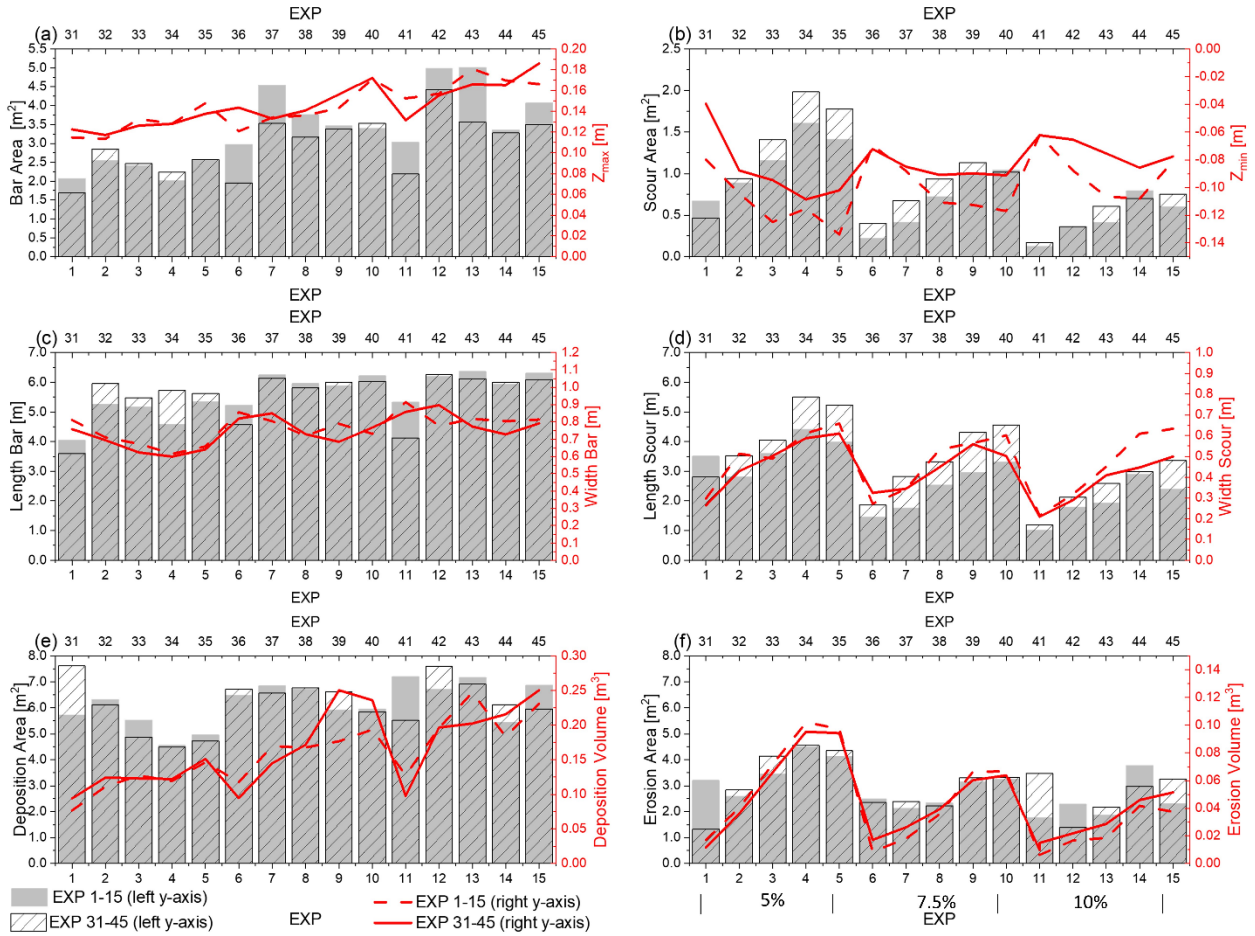

EXP [10% tributary gradient, 90° confluence angle]	EXP [10 % tributary gradient, 45° Confluence angle]	Q_m	Q_s
[-]	[-]	[l s^{-1}]	[l s^{-1}]
1, 6, 11	31, 36, 41	15	1.5
2, 7, 12	32, 37, 42	45	4.5
3, 8, 13	33, 38, 43	75	7.5
4, 9, 14	34, 39, 44	105	10.5
5, 10, 15	35, 40, 45	135	13.5

Figure 8 Comparison of morphological attributes across experiments with a 45° confluence angle (EXP 31-45) and experiments with a 90° confluence angle (EXP 1-15). Deposition bar and scour areas (a, b) are delineated by deposition or erosion above or below 0.01 m, respectively. The width and length values represent the maximum measured width or length (c, d), while the main channel deposition and erosion areas (e, f) represent all deposition and erosion in the main channel.

Figure 9 illustrates that variations in tributary depositional properties occurred despite maintaining a consistent tributary gradient across the experimental groups. When the confluence angle was 45° (EXP 31-45), a near overall increase in the depositional volume and a decrease in the depositional gradient was observed (Fig. 9) relative to experiments with a 90° confluence angle (EXP 1-15). A reduction in the confluence angle limits tributary channel flow penetration into the main channel (Best, 1988), reducing the exposure of the tributary sediment to main channel entraining forces. In the context of experiments 1-15, with a greater confluence angle (90°), the penetration of the tributary channel exhibited a greater extent. Increasing the confluence angle caused a greater mutual deflection of flows, further segregating the tributary and main channel flows (Best, 1987). This factor, coupled with the increased velocity, allowed the tributary sediment load to rapidly pass through the confluence zone when the confluence angle was 90° rather than be deposited in the tributary channel.

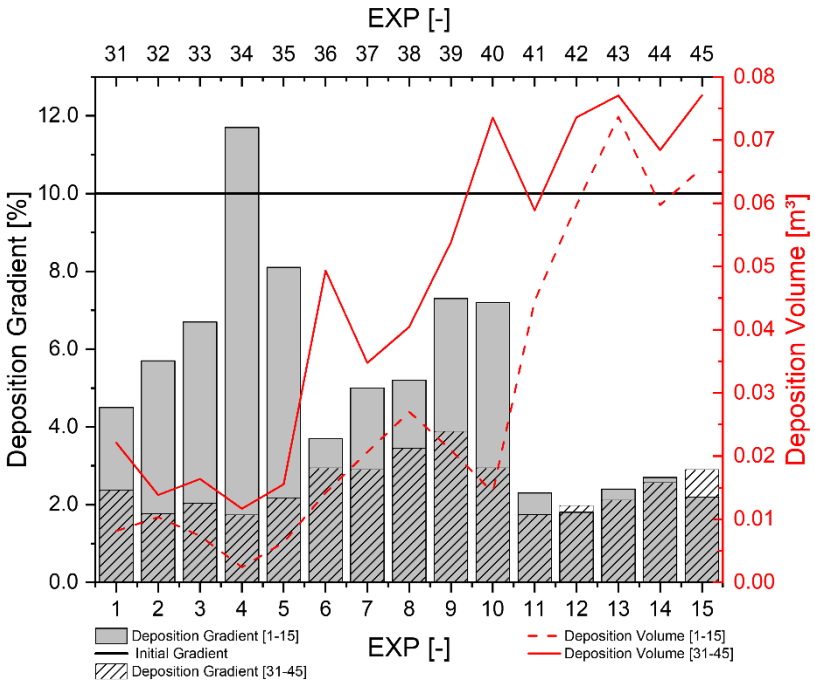

Figure 9 Gradients and volumes of deposited sediment in the tributary channel for experiments 1-15 (10% tributary gradient, 90° confluence angle) and 31-45 (10% tributary gradient, 45° confluence angle).

3.4 Statistical analysis of controlling factors impacting confluence morphology

3.4.1 Overview

Only controlling factors that had a significant effect (Table 5) on the response variables of the main channel are discussed. The focus of the statistical analysis was to determine the dominant controls over confluence morphology. For this reason, tributary channel depositional behavior was not included as a response variable.

Table 5 Introduced controlling factors and their impact on confluence morphology, bold text indicates the factor had a significant impact on one or more groups of the response variable. P-values from overall mean comparison tests are included.

Factor	z_{max}	z_{min}	Deposition area	Deposition volume	Erosion area	Erosion volume	Bar area	Bar length	Bar width	Scour area	Scour length	Scour width
Sediment concentration	**<.0001**	.30	.09	**.001**	.19	**.015**	**2.85E-4**	.059	**<.0001**	**4.38E-4**	**3.63E-4**	.30
Discharge	**.004**	**<.0001**	**.047**	**<.0001**	**.007**	**<.0001**	**1.89E-4**	**<.0001**	.14	**<.0001**	**<.0001**	**<.0001**
Tributary gradient	.20	.78	.82	.24	.96	.50	.27	.79	.21	.33	.35	.55
Confluence angle	.46	**0.022**	.91	.40	0.84	.67	.25	.81	.37	.23	**.047**	.267

3.4.2 Sediment concentration

Table 6 and Fig. 10 show that sediment concentration had a significant impact on 7 out of 12 response variables. Increased or decreased sediment concentration enhanced depositional or erosional patterns, respectively. Post hoc testing further revealed patterns caused by the sediment concentration (Table 6). Unsurprisingly, the majority of the significant differences in mean response values occurred between 5% and 10% sediment concentration groups. The maximum deposition depth was significantly reactive to all sediment concentrations. With increasing sediment concentration the deposition depth increased but reached a maximum as aggradation cannot exceed the local flow depth. When the sediment concentration was 7.5%, the response variables did not significantly differ from those of the 5% and 10% groups.

Table 6 Sediment concentration and its impact on the response variables; (σ) is the standard deviation. Pairwise post hoc mean comparison testing is summarized with letters A, B, and C. Means that do not share a letter are significantly different. For example, the mean Z_{max} for each sediment concentration group was significantly different (A, B, C), but the mean deposition volume for 7.5% and 10% sediment concentration groups did not significantly differ from each other (B, B) but were significantly different from the mean deposition volume when the sediment concentration was 5% (A).

	σ								
Response Variable	**5%**	**7.5%**	**10%**	**Test**	**Difference in Means**	**Post hoc Test**	**5**	**7.5**	**10**
[-]	**[-]**	**[-]**	**[-]**	**[-]**	**[-]**	**[-]**	**[%]**	**[%]**	**[%]**
Z_{max} [m]	0.01	0.02	0.02	ANOVA (F = 18.5)	Yes	Tukey-Test	A	B	C
Z_{min} [m]	0.02	0.02	0.02	ANOVA (F = 1.2)	No				
Deposition area [m^2]	1.00	0.68	0.85	ANOVA (F = 2.4)	No				
Deposition volume [m^3]	0.02	0.05	0.06	ANOVA (F = 8.2)	Yes	Tukey-Test	A	B	B
Erosion area [m^2]	1.02	0.74	0.87	ANOVA (F = 1.7)	No				
Erosion volume [m^3]	0.03	0.02	0.01	Welch ANOVA (F = 4.9)	Yes	Games-Howell	A	A/B	B
Deposition bar area [m^2]	0.47	0.72	1.01	Welch ANOVA (F = 11.5)	Yes	Games-Howell	A	B	B
Length bar [m]	0.88	0.57	0.74	ANOVA (F = 3.0)	No				
Width bar [m]	0.07	0.08	0.09	ANOVA (F = 13.3)	Yes	Tukey-Test	A	B	B
Scour area [m^2]	0.47	0.30	0.22	Welch ANOVA (F= 10.6)	Yes	Games-Howell	A	A	B
Length scour [m]	0.96	0.96	0.67	ANOVA (F = 9.7)	Yes	Tukey-Test	A	B	B
Width scour [m]	0.14	0.12	0.14	ANOVA (F = 1.3)	No				

Adjustments in deposition and erosion areas allowed for the majority of the incoming sediment load to pass through the confluence. However, given the differences in sediment loads, rapid mutual adjustments were morphologically represented by the same general patterns but with less erosion and more aggradation as sediment concentration increased. The differences in mean response values between the experiments with 5% and 10% tributary sediment concentrations and the similarities to the mean response values, when the sediment concentration was 7.5%, can be attributed to this process.

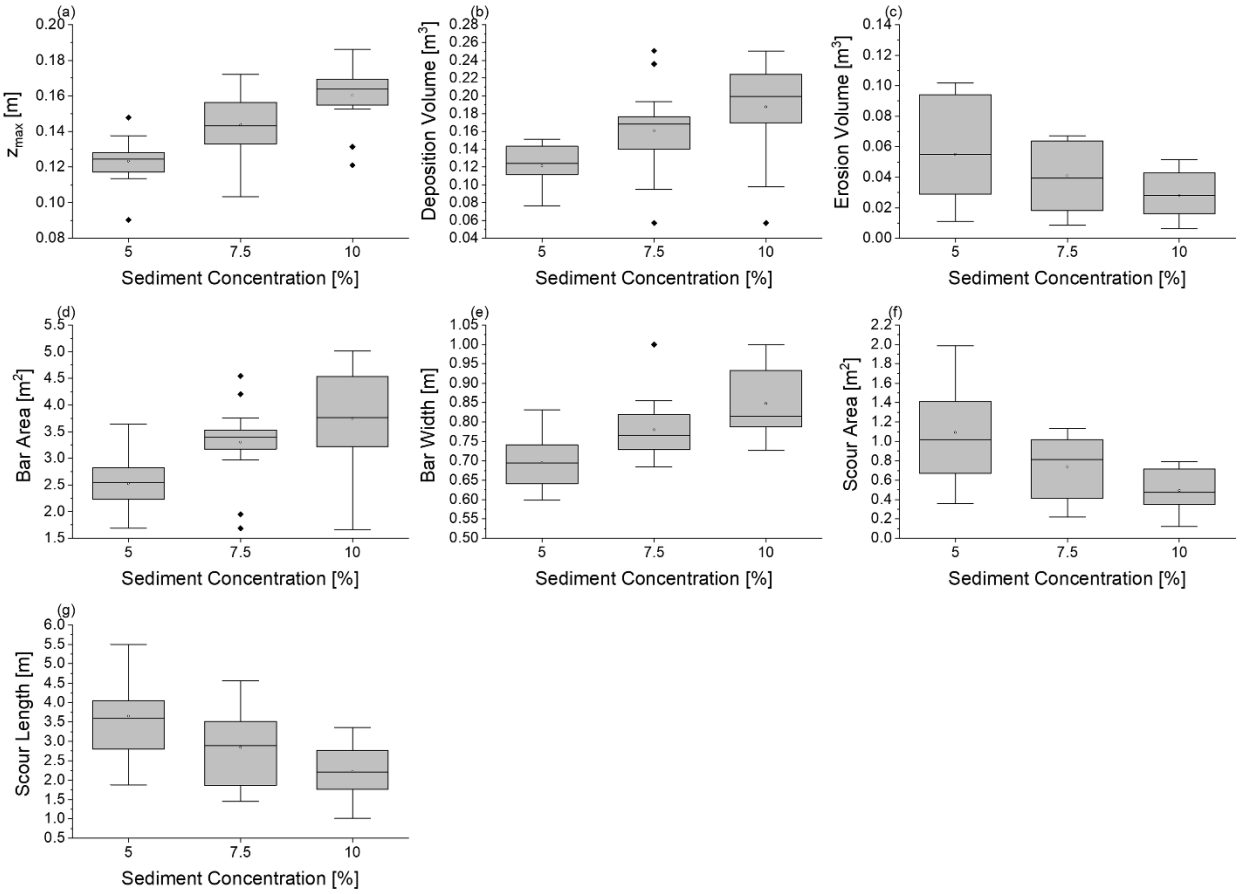

453

454 **Figure 10** Boxplots from ANOVA and Welch ANOVA results for all response variables that showed a
455 significant difference in mean values (Table 5) with sediment concentration as the controlling factor.

456

457 **3.4.3 Combined discharge**

458

459 Table 7 and Fig. 11 show that the discharge significantly affected 11 out of 12 response variables. Generally,
460 erosional processes increased with increasing discharge as the transport capacity of the main channel flow
461 increased. At lower discharges with limited transport capacity, erosional processes were comparatively
462 reduced. However, certain instances revealed increased depositional properties with increasing discharge
463 (Fig. 11a and 11d). This most apparently occurred between the 16.5 l s^{-1} and 49.5 l s^{-1} combined discharge
464 experiments. A deposition cone formed across all sediment concentrations when the combined discharge
465 was 16.5 l s^{-1}. Unlike the bar or transitional morphology, the deposition cone does not occupy the separation

zone and is characterized by a short longitudinal extent while protruding furthest into the main channel from the tributary channel. At discharges at and above 49.5 l s^{-1}, the depositional patterns shifted, and sediment was entrained and deposited in the separation zone. The separation zone is the largest sink for tributary-transported sediment; the occupying bar can only be as big as the hydraulic zone, which is the same size for a given discharge ratio (Best, 1987; 1988). This explains the subtle differences in depositional properties once the combined discharge exceeded 49.5 l s^{-1}.

Table 7 Discharge and its impact on the response variables; (σ) is the standard deviation. Pairwise post hoc mean comparison testing is summarized with letters A, B, C, and D; means that do not share a letter are significantly different.

	σ												
Response Variable	**16.5**	**49.5**	**82.5**	**115.5**	**148.5**	**Test**	**Diff. in means**	**Post Hoc Test**	**16.5**	**49.5**	**82.5**	**116**	**149**
[-]	**[l s^{-1}]**	**[l s^{-1}]**	**[l s^{-1}]**	**[l s^{-1}]**	**[l s^{-1}]**	**[-]**	**[-]**	**[-]**	**[l s^{-1}]**	**[l s^{-1}]**	**[l s^{-1}]**	**[l s^{-1}]**	**[l s^{-1}]**
Z_{max} [m]	0.02	0.02	0.02	0.02	0.02	ANOVA (F = 4.5)	YES	Tukey-Test	A	A/B	A/B	A/B	B
Z_{min} [m]	0.01	0.01	0.02	0.01	0.02	ANOVA (F = 10.7)	YES	Tukey-Test	A	B	B	B	B
Deposition [m^2]	1.07	0.52	0.93	0.77	0.68	ANOVA (F = 2.7)	YES	Tukey-Test	A	A	A	A	A
Deposition [m^3]	0.02	0.03	0.04	0.04	0.05	ANOVA (F = 9.3)	YES	Tukey Test	A	B	B	B	B
Erosion area [m^2]	1.08	0.52	0.92	0.66	0.63	ANOVA (F = 4.1)	YES	Tukey Test	A	A	A/B	B	A/B
Erosion volume [m^3]	0.004	0.01	0.02	0.02	0.02	Welch ANOVA (F = 28.9)	YES	Games-Howell	A	B	B/C	C	C
Bar area [m^2]	0.52	0.91	0.79	0.71	0.54	ANOVA (F= 7.2)	YES	Tukey Test	A	B	B	B	B
Length bar [m]	0.62	0.33	0.38	0.5	0.34	ANOVA (F = 22.0)	YES	Tukey Test	A	B	B	B	B
Width bar [m]	0.06	0.11	0.11	0.12	0.06	ANOVA (F = 1.9)	NO						
Scour area [m^2]	0.17	0.24	0.33	0.42	0.38	ANOVA (F = 9.1)	YES	Tukey Test	A	A/B	B/C	C	C
Length scour [m]	0.8	0.63	0.76	0.92	0.87	ANOVA F = 8.4)	YES	Tukey Test	A	A	A/B	B	B
Width scour [m]	0.05	0.08	0.06	0.06	0.06	ANOVA (F = 36.9)	YES	Tukey Test	A	B	C	D	D

Pair-wise post hoc comparisons of maximum deposition depth indicated a significant difference in mean values between the lowest and highest combined discharge experiments while revealing similarities among intermediate discharge scenarios. These similarities could be attributed to the combined flows regulating the depositional depth, which does not exceed the flow depth. The observed differences can be attributed to the increased sediment load and associated morphological changes with increasing discharge.

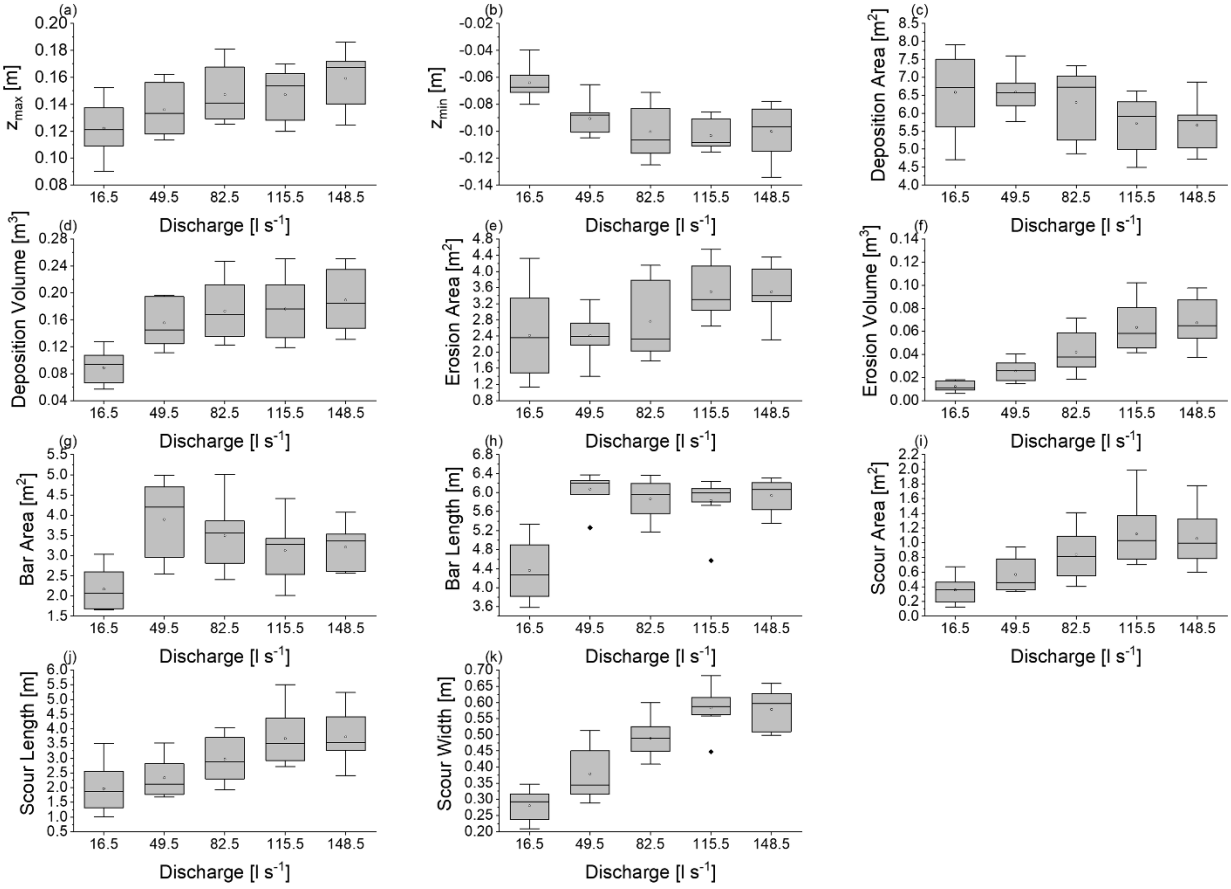

Figure 11 Boxplots from ANOVA and Welch ANOVA results for all response variables that showed a significant difference in mean values (Table 5) with combined discharge as the controlling factor.

3.4.4 Confluence angle

Surprisingly, the confluence angle only had a significant influence on 2 out of the 12 response variables (Table 8). The confluence angle did have a decisive impact on scour depth (Fig. 12a). This could be attributed to the degree of turbulence increasing with increasing confluence angle (Mosley, 1976). The elevated turbulence arises from the increased mutual flow deflection, which influences the shear layers generated between the two converging flows. Along these shear layers, powerful vortices are created which enhance the bed shear stress within the junction, resulting in significant bed scour (Best, 1987). Reducing the confluence angle allowed for improved mixing of tributary and main channel flows, which in turn decreased the turbulence in the confluence producing shallower scour.

Table 8 Confluence angle and its impact on the response variables. Post hoc testing was not required since there are only two groups to compare; σ is the standard deviation.

	σ			
Response Variable	**45°**	**90°**	**Test**	**Difference in means**
[-]	**[-]**	**[-]**	**[-]**	**[-]**
Z_{max} [m]	0.02	0.02	T-Test (t statistic = - 0.742)	NO
Z_{min} [m]	0.02	0.02	T Test (t statistic = -2.37)	YES
Deposition Area [m^2]	0.96	0.85	T Test (t statistic = 0.109)	NO
Deposition Volume [m^3]	0.06	0.05	T Test (t statistic = -0.843)	NO
Erosion Area [m^2]	0.98	0.87	T Test (t statistic = -0.199)	NO
Erosion Volume [m^3]	0.03	0.03	T Test (t statistic = -0.425)	NO
Deposition Bar Area [m^2]	0.75	0.95	T Test (t statistic = 1.169)	NO
Length Bar [m]	0.81	0.77	T Test (t statistic = 0.238)	NO
Width Bar [m]	0.10	0.10	T Test (t statistic = 0.916)	NO
Scour Area [m^2]	0.52	0.36	T Test (t statistic = -1.212)	NO
Length Scour [m]	1.22	0.88	T Test (t statistic = -2.04)	YES
Width Scour [m]	0.12	0.14	T Test (t statistic = 1.125)	NO

Additionally, the confluence angle had an impact on the length of the scour (Fig. 12b). Enhanced mixing of confluent flows and a reduced hydraulic separation zone created conditions where the scour generally occupied a greater area but produced a shallower scour depth. However, the width of the bar was relatively unchanged (Fig. 8c) in response to the confluence angle; the increased scour area was represented by an increase in scour length. While the penetration of the tributary channel was reduced, the transport capacity of the main channel was still sufficient to mobilize a similar volume of sediment (Fig. 8f).

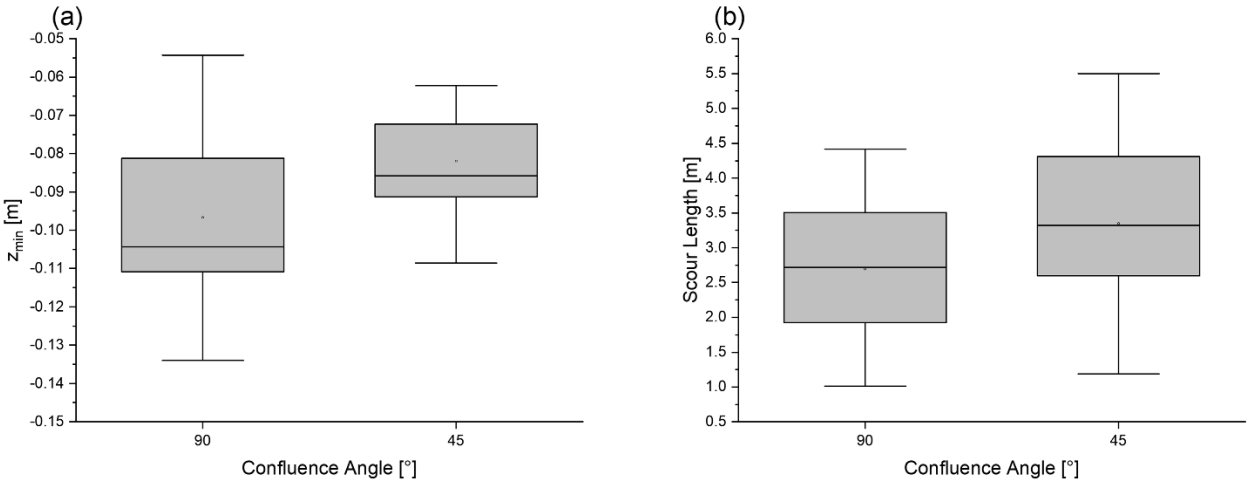

Figure 12 Boxplots from T-Test results for all response variables that showed a significant difference in mean values (Table 5) with the confluence angle as the controlling factor.

4 Discussion

4.1 Special dynamics of mountain river confluences

The confluence angle has been established as one of the main drivers of confluence morphology, thus affecting the spatial distribution of the hydraulic zones for lowland confluences. However, for mountain river confluences during events with intense bedload transport it had a minimal effect, corroborating hypothesis 1, that adjustments to the confluence angle (Fig. 8, Table 8) and the tributary gradient (Fig. 5, Table 5) do not significantly impact confluence morphology and the development of specific geomorphic units. Wohl (2010) discusses the extremal hypotheses (Davies & Sutherland, 1983) which are based on the underlying assumption that the equilibrium channel morphology corresponds to the morphology that maximizes or minimizes the value of a specific parameter (Darby and Van De Wiel, 2003). Examples of this are reductions of unit stream power (Yang & Song, 1979) and energy dissipation rate (Yang, 1976) and maximizations of friction factor (Davies and Sutherland, 1983), and sediment transport rate (White et al., 1982). The confluence morphologically reacted to the steep channel flooding and bedload conditions, characterized by higher velocities, sediment concentrations, and Froude numbers than what would be expected at a lowland confluence, and adjusted to maximize sediment transport through the confluence. Since all channel geometry experiments were exposed to the same discharges and sediment supply rates, a similar development occurred. Lowland regions are typically less intense and morphologically more responsive, relative to mountain river confluences during flooding events, to variations in the size and orientation of the hydraulic zones as they respond to channel adjustments (Mosley, 1976; Best 1987, 1988; Liu et al., 2015). Scour area and depth were the only response variables sensitive to the confluence angle. Decreasing the confluence angle limited the extent of the flow separation zone (Mosley, 1976; Best, 1987). The zone of maximum velocity responded to the size of the flow separation zone (Best, 1987). When more channel was available for the zone of maximum velocity from the decreased size of the separation zone, the velocity decreased, causing shallower scour, which is consistent with the findings of Mosley (1976) and Best (1988). In contrast, increasing the confluence angle increased the local velocity and transport capacity and caused greater penetration of the tributary flow. These combined aspects provide evidence that the transport capacity of the main channel is enhanced at higher confluence angles, which was reflected in the tributary depositional volumes and gradients. It has been previously observed in mountain rivers (Mueller & Pitlick,

2005; Trevisani et al., 2010) that the tributary channel gradient responds to the transport capacity of the flow. Mueller and Pitlick (2005) suggest that forced changes in gradient are offset by adjustments to width, depth, and bed surface texture to maintain a balance between the intensity and frequency of bed load transport. In confined channels, width adjustments are not possible, resulting in extensive deposition in the channel. The main differences in sediment depositional patterns and mechanisms from adjusting the tributary channel gradient were observed in the tributary channel, while the main channel was largely unchanged. This indicates that with a sustained and abundant sediment supply and relatively uniform main channel hydraulic conditions, the morphologic development of the confluence is not significantly impacted by changes in the tributary channel gradient.

Referring to hypothesis 2 (sediment concentration and channel discharge exert the most control over depositional and erosional patterns), the same geomorphic units and morphological patterns occurred for all experimental groups and channel configurations, which establishes the dominance of the combined channel discharge over the confluence. This can be explained according to Guillén-Ludeña et al., (2017) where the main channel supplies the dominant flow discharge. The unit stream power in the main channel (Table 4) was sufficient to force the development of the same geomorphic units, for a specific discharge, regardless of changes to sediment concentration and channel geometry. Adjustments to sediment concentration were reflected in varying ranges of deposition and erosion depths and volumes, as well as varying extents of these geomorphic units. Interaction between discharge and sediment shows clear trends of coarsening or fining at specific sites (Fig. 13, Appendix 10) for all the introduced controlling factors. However, trends relating sediment concentration or channel geometry to coarsening or fining are not apparent since the same general morphological patterns consistently occurred, which in turn caused similar hydraulic conditions to develop. Grain size distribution curves from the tributary channel near the confluence, the deposition cone or bar, and the recovery zone further illustrate the selective bedload transport occurring in the confluence zone. Consistent across all experiments, the deposited material in the tributary was finer than the input mix (Fig. 13a to 13c, Appendix 10). For experiments with the 10% tributary gradient, this can be explained by the regressive aggradation occurring in the tributary channel, which reduced the gradient of the tributary and, thus, its transport capacity. For experiments with a 5% tributary gradient, the transport capacity of the tributary was saturated, which caused intense progressive deposition of all grain sizes in the channel despite the increased depositional gradient. Samples taken from the scour

hole (Fig. 13d to 13f, Appendix 10) showed an overall coarsening, illustrating the enhanced transport capacity through this zone. The separation zone bar was formed in a region of low flow velocity relative to the main channel, which is reflected in the associated grain size distributions (Fig. 13h and 13i, Appendix 10). The samples taken from the lowest discharge experiments were from the deposition cone; the cone did not occupy the hydraulic separation zone and was exposed to the main channel flow. Accordingly, the samples showed a general coarsening pattern of the finer grain fractions and a fining of the larger grain size fractions (Fig. 13g, Appendix 10). The zone of flow recovery is characterized by decreased turbulence and more uniform flow patterns and bed morphology (Best, 1987; 1988). As a result, no hydraulic or morphologic structures existed that influenced the velocity distribution throughout this portion of the channel. This is apparent in Fig. 13j to 13l where the samples taken across all experiments showed the least deviation from the plotted line of the input material. A slight but overall coarsening is apparent, caused by the increased velocity from the combined channel flow and the resulting selective bedload transport.

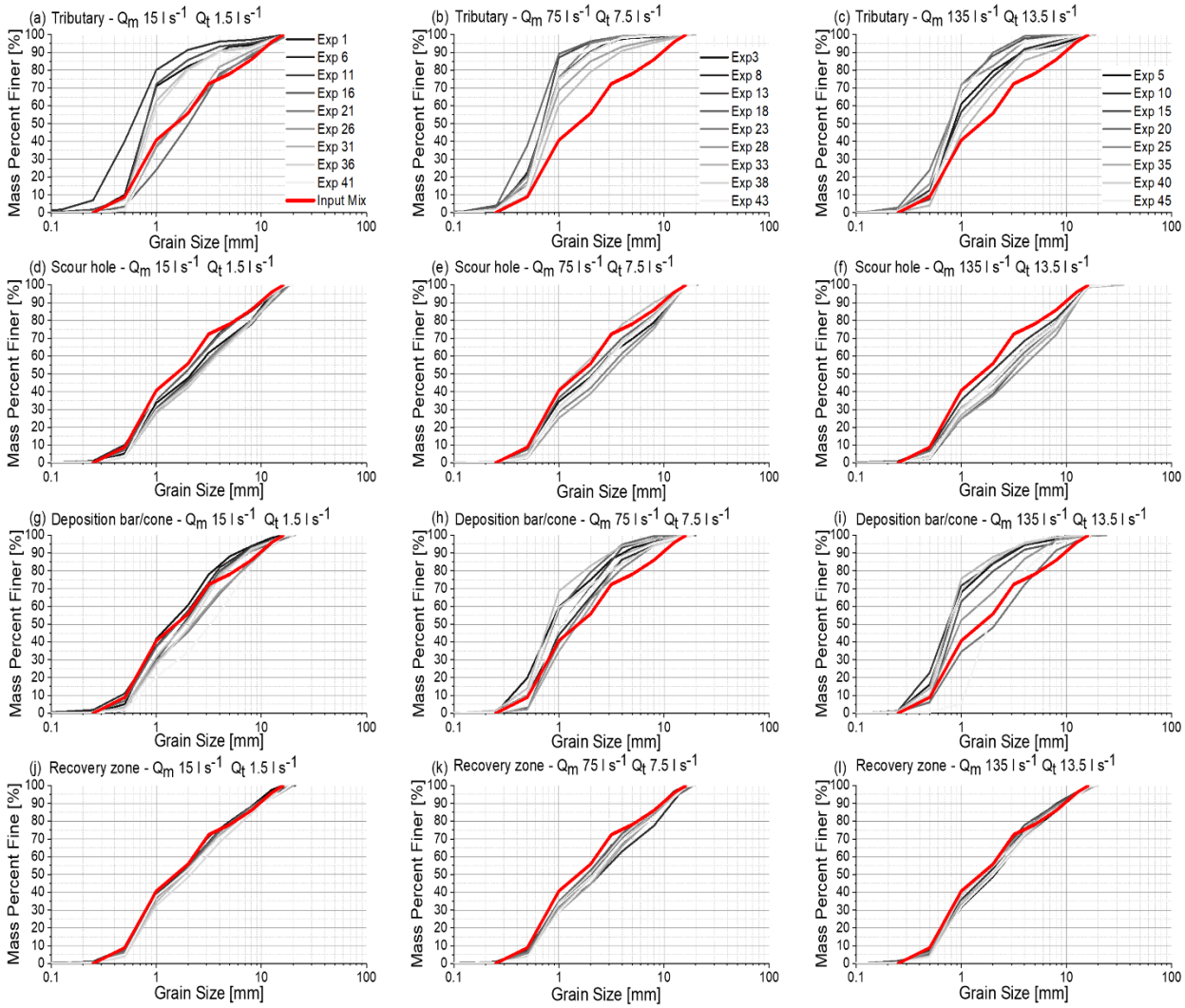

Figure 13 Grain size distribution curves from samples taken from the tributary channel (a-c), the scour hole (d-f), the deposition cone or bar (g-i), and the recovery zone (j-l) for the lowest, middle, and highest experimental discharges, Q_m and Q_t denote main and tributary channel discharges, respectively.

4.2 Modelling limitations

Modelling limitations deal mainly with scale effects and the duration required to set up and run an experiment, limiting the scope of the study, but creating a well-founded base to build from. Preparing and running an experiment took multiple days; the project duration did not allow investigations into the effects of the discharge ratio. An ideal experimental program would have included the same 45 experiments but with a different discharge ratio. Accordingly, we strongly encourage additional investigations into this

component as it influences mountain river confluences. All physical models are subject to some degree of scale effects as it is impossible to correctly model all force ratios (Chanson, 2004; Heller, 2011). This arises from having to choose the most relevant force ratio, which for open channel hydraulics is Froude similarity (Heller, 2011). Under Froude similarity, the remaining force ratios cannot be identical between model and prototype and can result in non-negligible scale effects (Heller, 2011). Scale effects generally increase with increasing prototype to model scale factor (Heller, 2011). Scale limitations of grain size diameters are discussed in Zarn (1992), where grain sizes smaller than 0.22 mm can change the flow-grain interaction due to cohesion effects. In this regard, Oliveto and Hager (2005) discuss limiting the D_{50} to 0.80 mm. The model grain size distribution has a minimum grain size of 0.5 mm and a D_{50} of 1.4 mm. The Shields (θ) number and the grain Reynolds (Re^*) number were calculated in the main channel for all discharges and geometric configurations. At the lowest discharge experiments, θ and Re^* at the model scale range from 0.08-0.10 and 60-67, respectively. At prototype scale Re^* ranges from 9849-10927. At the next discharge combination, θ and Re^* at the model scale range 0.15-0.17 and 82-87, respectively. At prototype scale Re^* ranges from 13523-14247. While there is certainly a significant shift in Re^* between lab and prototype scales, Aufleger (2006) states that assuming Froude similarity and minimizing scale effects for pre-alpine gravel bed rivers Re^* numbers at the model scale above 80 are recommended. In this regard, for the lowest discharge experiments, the smaller grain fractions were subject to some degree of scale effects.

5 Conclusion

The channel discharges and then the tributary sediment concentration are the most impactful factors influencing mountain river confluence morphology during events with intense bedload transport. This conclusion contrasts with the findings of the literature dealing with the controls of river confluences. Mountain river confluences are influenced by characteristics unique to mountain regions, including the availability of massive amounts of sediment and frequent and intense localized flooding. The rate of sediment entering the confluence saturated the transport capacity of the main channel. The resulting morphologies represented a system tending towards an equilibrium state, optimized to maximize sediment transport through the confluence through local increases in sediment transport rate. Every geometric group

of experiments had the same discharges and sediment supply rates; the resulting morphologies were similar because the channel was responding to similar intense hydraulic and sediment supply conditions. This limited the effect the channel adjustments had on the hydraulic zones influencing confluence morphology. However, adjustments did cause an apparent response to the depositional mechanisms in the tributary channel. A progressive or regressive aggradation of tributary sediment occurred, which enhanced or reduced the tributary channel transport capacity. Rapid mutual adjustments occurred as the system tended towards an equilibrium state. The evolution towards an equilibrium morphology was characterized by the geomorphic units, which reflected the flood magnitude. With increasing discharge, the geomorphic units transitioned from a cone to a bank-attached bar as the depositional patterns were forced further downstream and into the separation zone, with the bank-attached bar occupying the full extent of the separation zone. When sediment concentration was fixed, and the discharge was adjusted, the morphology responded to the combined channel flows downstream of the confluence. However, the morphological patterns were mainly unaffected when the discharge was fixed and the sediment concentration was adjusted. Therefore, the combined discharge determined the overall morphology and the development of specific geomorphic units, and the sediment concentration controlled the morphological extent of the units. These aspects illustrate that the morphological spatial patterns at mountain river confluences are unique and require special attention for flood risk management.

6 Appendix

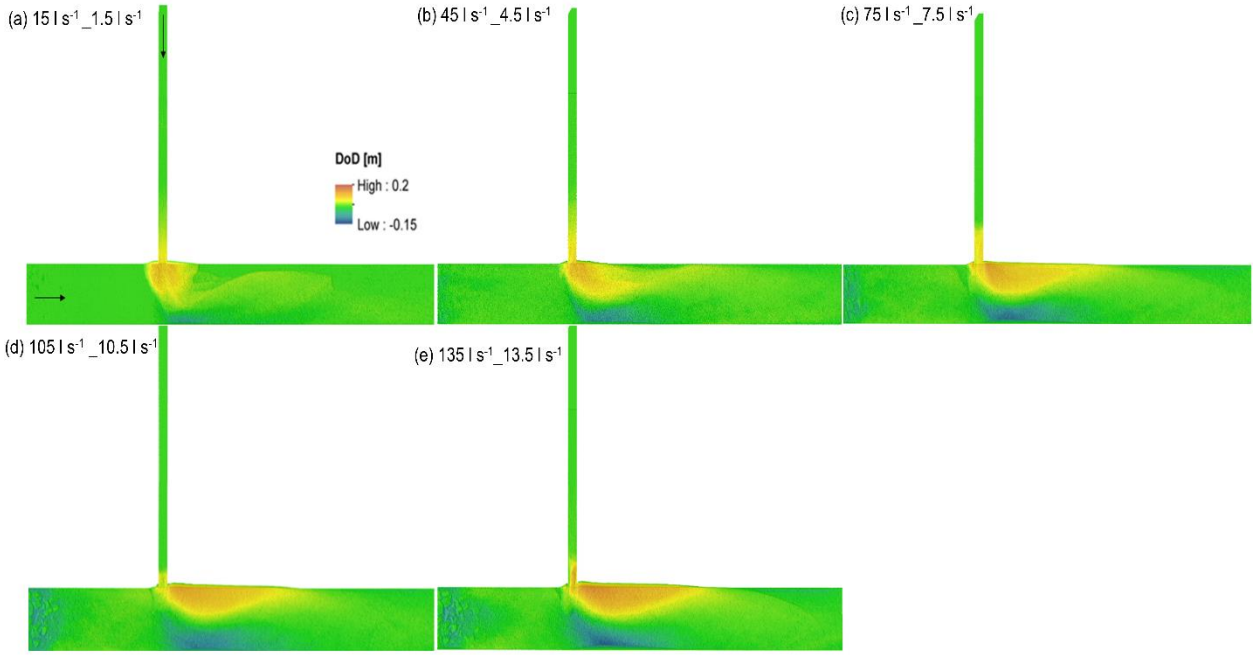

A 1 Confluence morphology for experiments 1-5 with 5% sediment concentration, a 90° confluence angle, and a 10% tributary gradient.

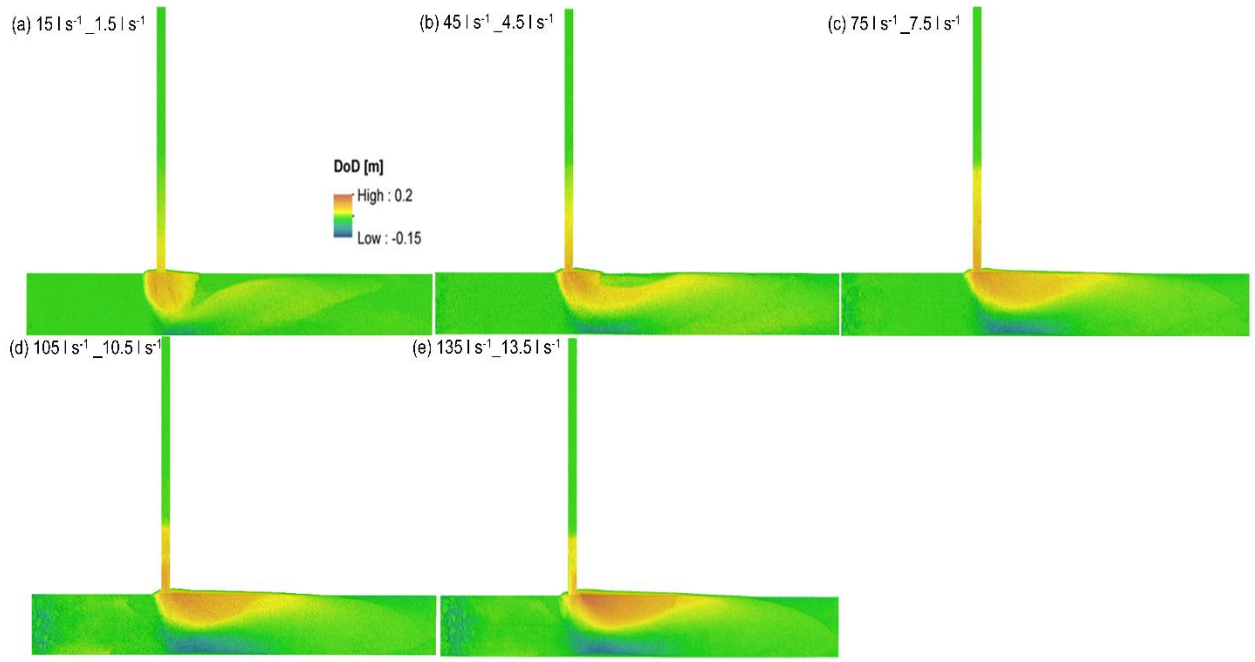

A 2 Confluence morphology for experiments 6-10 with 7.5% sediment concentration, a 90° confluence angle, and a 10% tributary gradient.

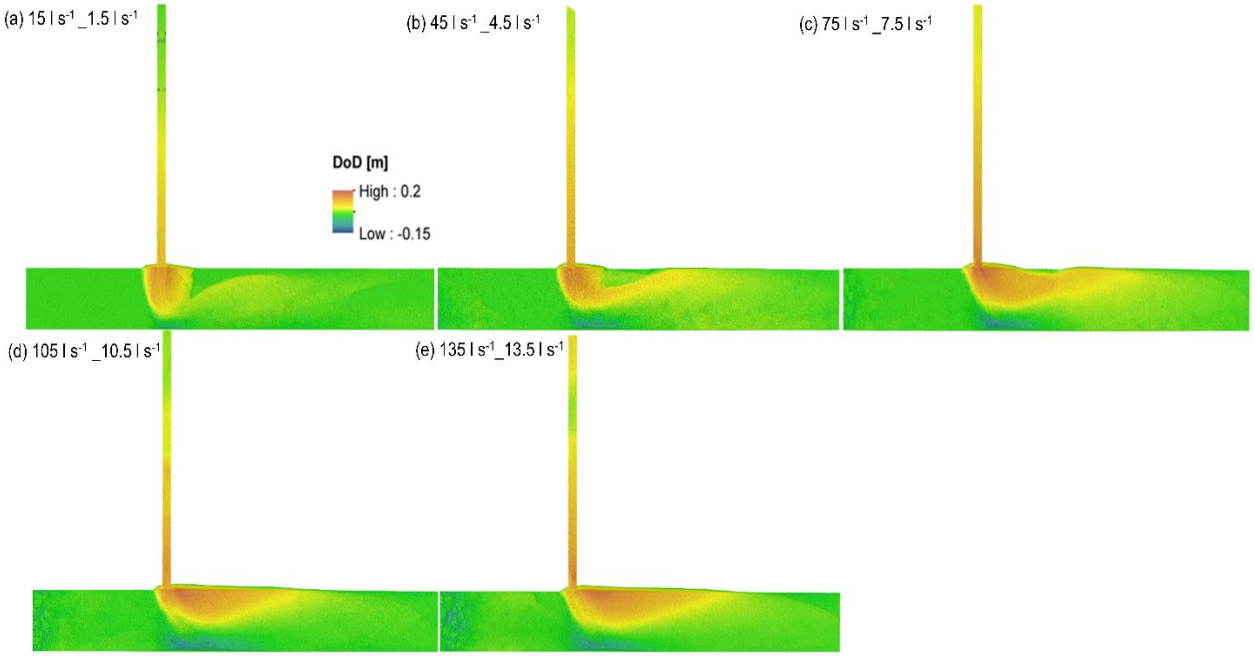

644

645 **A 3** Confluence morphology for experiments 11-15 with 10% sediment concentration, a 90° confluence

646 angle, and a 10% tributary gradient.

647

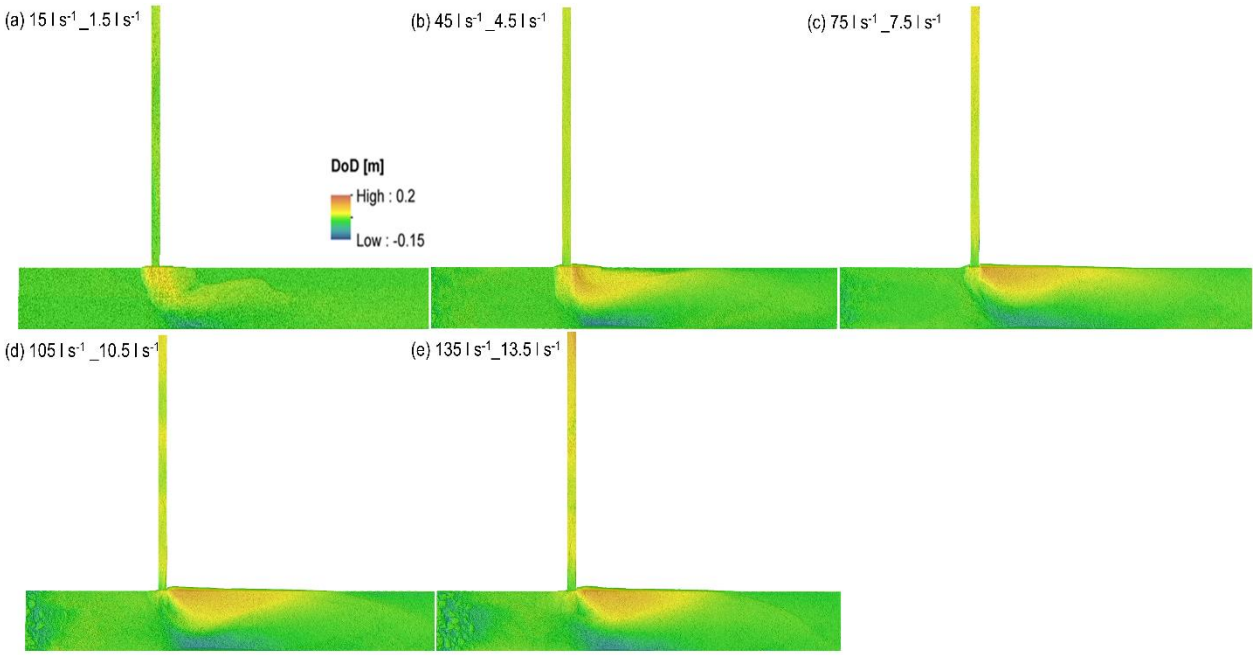

648

649 **A 4** Confluence morphology for experiments 16-20 with 5% sediment concentration, a 90° confluence

650 angle, and a 5% tributary gradient.

651

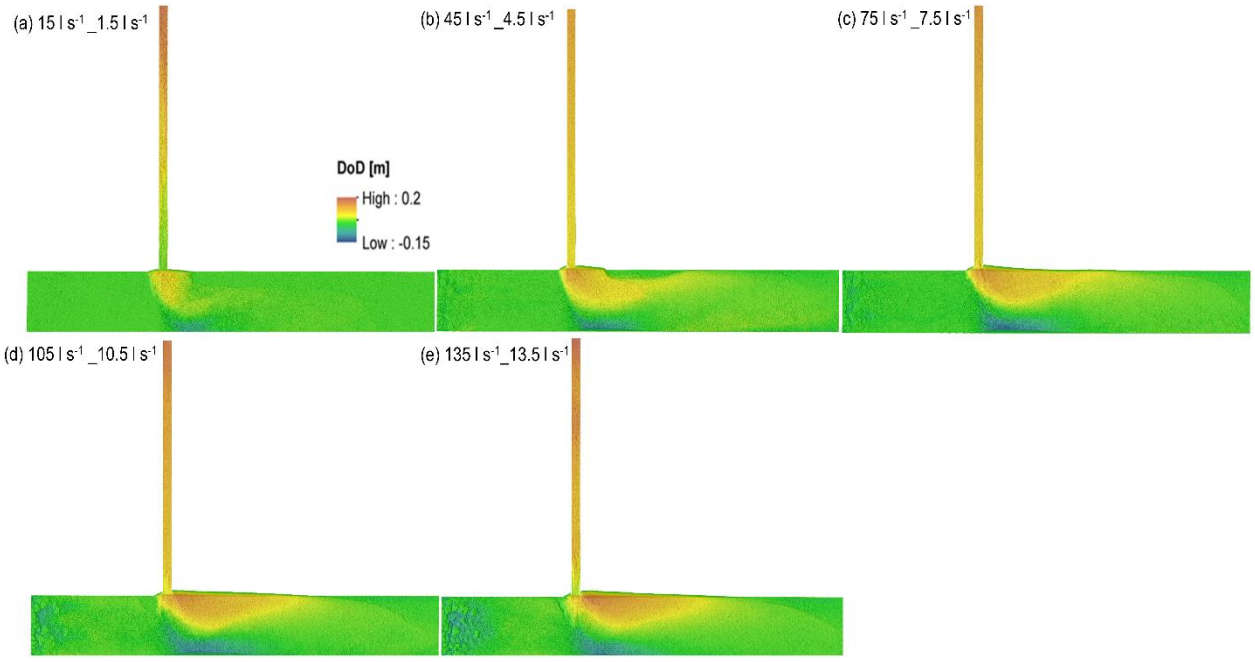

652

653 **A 5** Confluence morphology for experiments 21-25 with 7.5% sediment concentration, a 90° confluence

654 angle, and a 5% tributary gradient.

655

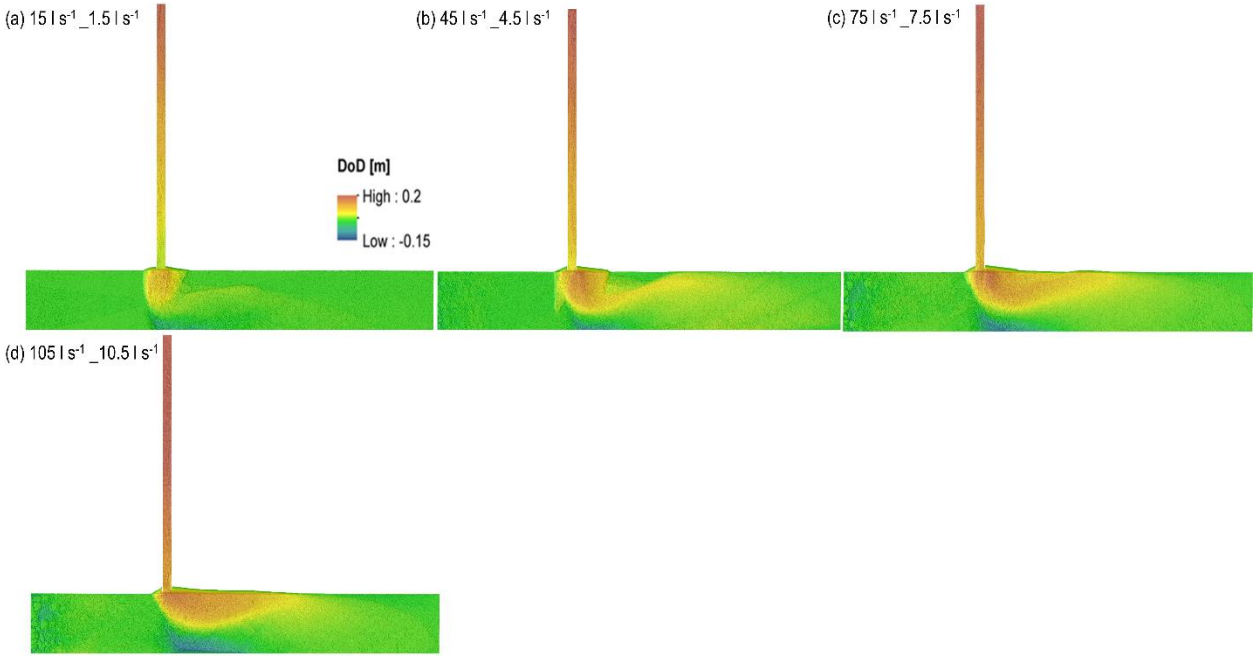

656

657 **A 6** Confluence morphology for experiments 26-29 with 10% sediment concentration, a 90° confluence

658 angle, and a 5% tributary gradient.

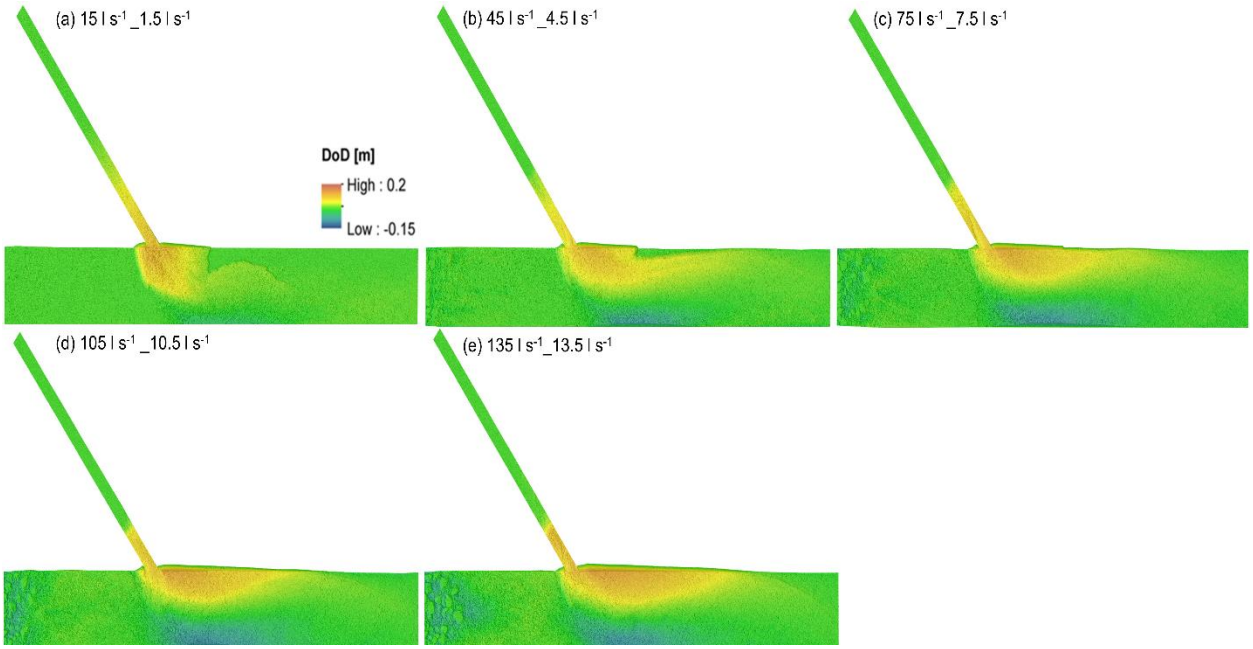

659

660 **A 7** Confluence morphology for experiments 31-35 with 5% sediment concentration, a 45° confluence

661 angle, and a 10% tributary gradient.

662

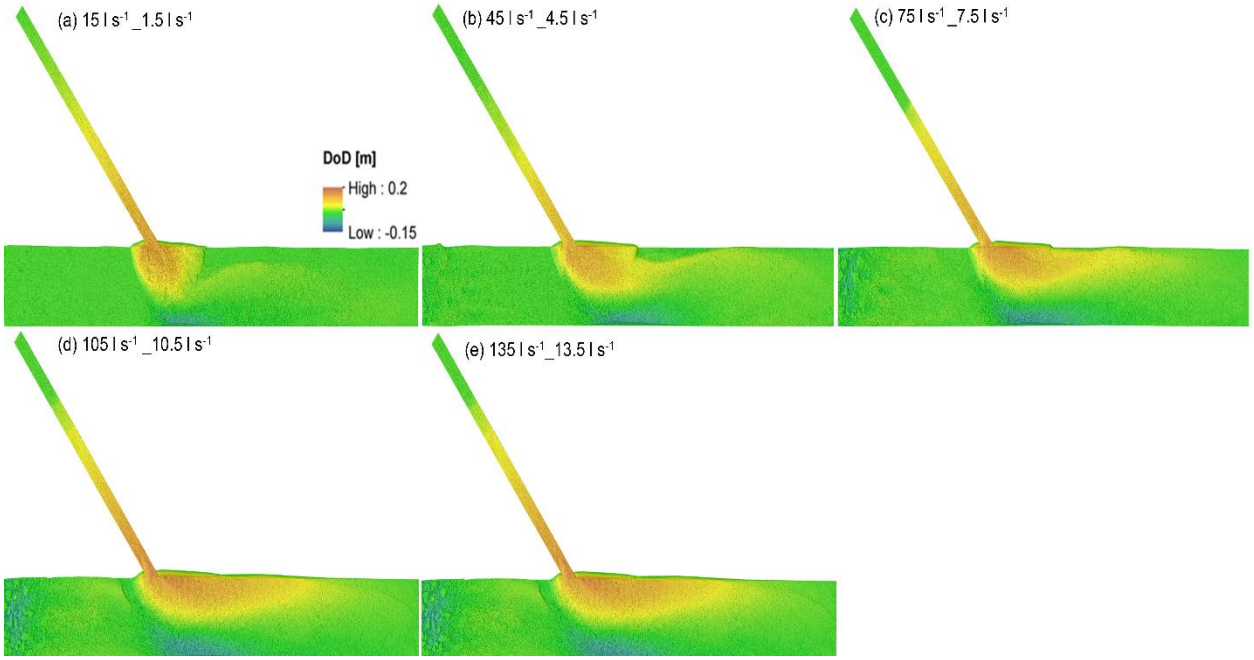

663

664 **A 8** Confluence morphology for experiments 36-40 with 7.5% sediment concentration, a 45° confluence

665 angle, and a 10% tributary gradient.

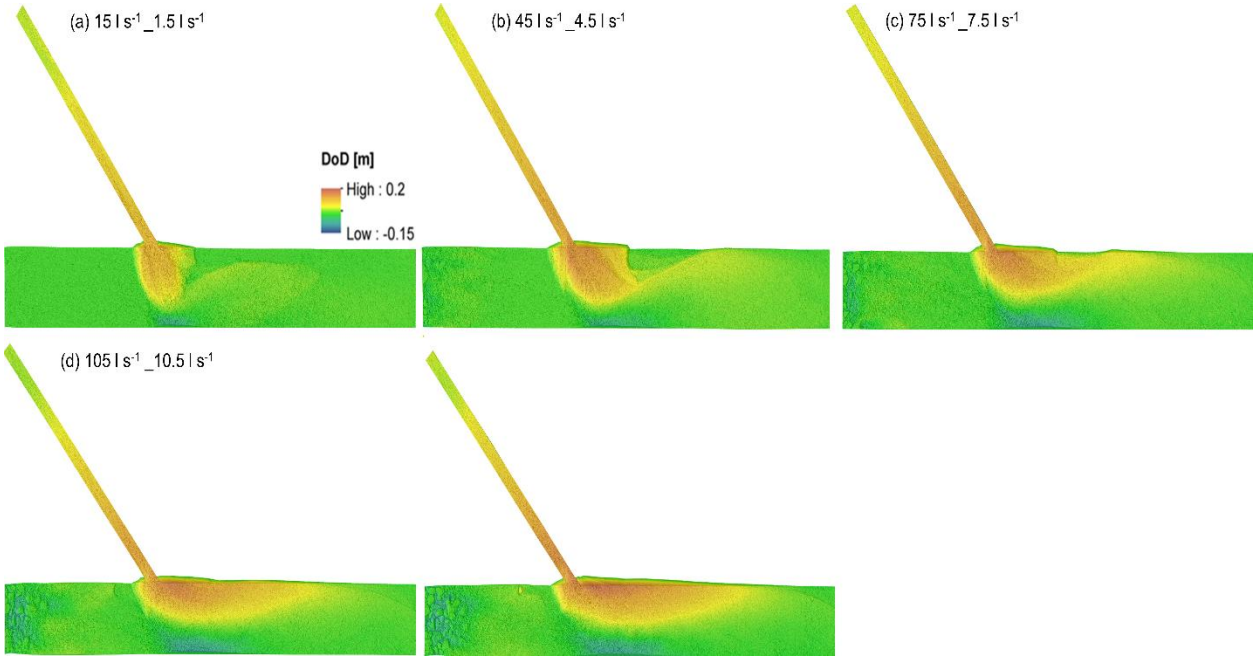

666

667 **A 9** Confluence morphology for experiments 41-45 with 10% sediment concentration, a 45° confluence

668 angle, and a 10% tributary gradient.

669 **A 10** Characteristic grain size for all experiments from samples taken in the tributary channel, the
670 geomorphic units (depositional or scour hole), and the recovery zone. Bold text indicates that the sampled
671 grain size was larger than the input mix grain size.

Exp	D16				D50				D84				Dm			
	Trib.	Depo.	Scour	Recov.	Trib.	Depo.	Scour	Recov.	Trib.	Depo.	Scour	Recov.	Trib.	Depo.	Scour	Recov.
[-]	[mm]	[mm]	[mm]	[mm]	[mm]	[mm]	[mm]	[mm]	[mm]	[mm]	[mm]	[mm]	[mm]	[mm]	[mm]	[mm]
Input	0.7	0.7	0.7	0.7	1.4	1.4	1.4	1.4	6.2	6.2	6.2	6.2	2.8	2.8	2.8	2.8
1	0.5	0.6	0.7	0.6	0.8	**1.4**	**2.2**	**1.7**	2.4	4.3	**9.2**	6.2	1.8	2.5	**4.0**	**3.0**
2	0.5	0.6	0.7	0.6	0.9	**1.7**	**2.1**	**1.5**	2.5	5.6	**9.4**	**6.5**	1.5	**2.9**	**4.1**	**3.1**
3	0.4	0.5	0.7	0.5	0.8	0.9	**2.2**	1.4	1.6	2.9	**9.6**	6.0	1.1	1.8	**4.1**	**2.9**
4	0.5	0.5	0.6	0.6	0.9	0.9	**1.7**	1.4	3.7	2.9	**8.6**	**6.5**	2.6	1.9	**3.8**	**3.3**
5	0.6	0.5	0.7	0.6	0.9	0.8	**2.5**	1.3	2.8	2.0	**10.0**	6.2	2.0	1.5	**4.4**	**3.2**
6	0.3	0.6	0.6	0.6	0.6	**1.6**	**1.9**	**1.7**	1.3	4.7	**7.6**	**6.2**	1.2	**2.8**	**3.6**	**3.4**
7	0.4	0.6	**0.8**	0.6	0.7	1.0	**3.4**	**1.6**	0.9	3.2	**12.3**	**6.5**	0.8	2.0	**5.7**	**3.2**
8	0.4	0.6	0.6	0.5	0.8	1.3	**2.0**	1.2	1.6	3.8	**9.1**	6.0	1.1	2.4	**4.0**	**3.1**
9	0.6	0.6	**0.7**	0.6	0.9	0.9	**2.3**	**1.4**	1.9	3.7	**7.3**	**6.7**	1.4	2.5	**3.8**	**3.5**
10	0.5	0.4	0.7	0.7	0.9	0.8	**1.9**	**1.8**	3.0	2.0	**9.3**	**6.4**	1.9	1.3	**4.0**	2.4
11	0.6	**0.8**	**0.7**	**0.7**	0.8	**1.8**	**2.4**	**2.3**	1.9	5.3	**10.3**	**9.1**	1.7	**3.0**	**4.5**	**4.2**
12	0.5	0.7	**0.7**	**0.7**	0.8	**1.6**	**2.8**	**3.0**	2.6	3.9	**11.2**	**11.2**	1.6	2.6	**5.0**	**3.2**
13	0.5	0.6	**0.9**	0.7	0.7	1.1	**5.8**	**1.5**	1.0	3.2	**13.1**	**7.2**	0.9	1.9	**6.8**	**3.4**
14	0.4	0.6	**0.8**	0.6	0.8	1.3	**5.4**	1.3	1.9	3.4	**13.0**	4.4	1.3	2.1	**6.6**	2.7
15	0.6	0.6	**0.8**	0.7	0.8	0.9	**3.1**	**1.6**	1.8	2.7	**11.0**	6.1	1.2	1.8	**5.0**	**3.8**
16	**0.8**	0.6	0.7	0.6	**2.0**	**1.7**	**1.9**	**1.7**	**6.4**	5.6	3.4	**6.4**	**3.5**	**3.2**	**3.8**	**3.2**
17	0.4	0.7	**0.9**	0.7	0.7	**1.7**	**4.1**	**1.8**	0.9	5.2	3.8	**6.8**	0.7	**2.9**	**5.9**	**3.6**
18	0.3	0.6	0.6	0.6	0.6	0.9	**1.9**	**1.6**	1.0	2.6	3.7	6.0	0.8	1.5	**3.8**	**3.1**
19	0.4	0.6	**0.8**	0.7	0.7	**1.4**	**3.3**	**1.8**	1.0	5.3	3.8	**7.0**	0.9	**2.8**	**5.1**	**3.5**
20	0.4	0.7	0.7	0.6	0.8	**2.2**	**2.6**	1.4	1.7	**6.4**	3.9	**6.4**	1.1	**3.4**	**4.6**	**3.1**
21	**0.7**	**0.7**	**0.7**	0.7	**1.7**	**2.4**	**2.5**	**2.0**	**6.4**	**7.6**	3.6	**7.9**	**3.2**	**3.9**	**4.4**	**3.7**
22	0.5	**0.8**	**0.8**	0.7	0.7	**1.9**	**3.3**	**1.7**	1.0	4.9	4.1	**6.6**	0.9	**3.0**	**5.8**	**3.3**
23	0.4	0.7	**0.7**	0.6	0.8	**1.4**	**2.8**	**1.6**	1.4	4.8	3.8	**7.1**	1.0	2.7	**4.7**	**3.4**
24	0.5	0.6	0.7	0.6	0.8	1.3	**2.4**	**1.6**	1.6	4.3	3.7	6.0	1.1	2.6	**4.3**	**3.3**
25	0.5	0.6	**0.8**	0.6	0.8	1.0	**3.4**	**1.7**	2.2	3.7	3.8	**6.8**	1.4	2.1	**5.3**	**3.4**
26	**0.7**	**0.8**	**0.7**	0.7	**1.6**	**2.3**	**2.6**	**2.0**	5.0	**7.8**	3.8	**7.7**	**2.9**	**4.0**	**4.8**	**3.8**
27	0.5	**0.9**	**0.8**	0.7	0.8	**2.3**	**3.1**	**1.7**	1.0	5.6	3.8	**6.8**	0.9	**3.3**	**5.1**	**3.4**
28	0.5	**0.7**	**0.8**	0.7	0.8	**1.6**	**3.1**	**1.7**	1.9	3.7	3.9	**7.8**	1.5	2.4	**5.4**	**3.7**
29	0.5	0.7	**0.7**	0.7	0.8	**1.7**	**2.6**	**1.8**	1.8	5.9	3.8	**6.6**	1.3	**3.2**	**4.6**	**3.4**
30	-	-	-	-	-	-	-	-	-	-	-	-	-	-	-	-
31	0.6	**0.7**	**0.8**	0.7	0.9	1.9	**2.8**	**1.9**	2.6	5.7	**10.0**	**6.9**	2.0	**3.2**	**4.6**	**3.6**
32	0.5	0.5	0.7	0.7	0.8	0.9	**2.0**	**1.9**	1.7	3.5	**7.1**	**7.5**	1.2	2.1	**3.7**	**3.7**
33	0.6	0.52	0.7	0.7	0.9	0.8	**1.5**	**1.7**	2.8	2.2	6.0	**7.6**	1.9	1.5	**3.1**	**3.6**
34	0.6	0.6	**0.7**	0.7	0.9	0.9	**1.9**	**1.8**	2.9	3.5	**6.4**	**7.3**	1.8	2.1	**3.3**	**3.5**
35	0.6	0.5	**0.8**	0.7	1.2	0.8	**3.0**	**1.7**	3.8	1.7	**11.0**	**6.6**	2.6	1.3	**5.1**	**3.4**
36	0.6	**0.8**	**0.7**	0.7	0.9	**2.2**	**2.7**	**1.8**	2.8	5.9	**10.1**	**7.1**	2.1	**3.3**	**4.6**	**3.7**
37	0.5	0.7	0.7	0.7	0.8	**1.5**	**1.6**	**1.7**	1.7	5.9	**9.0**	**7.2**	1.2	**3.1**	**3.8**	**3.7**
38	0.5	0.6	**0.7**	0.6	0.8	0.9	**2.2**	**1.5**	1.6	4.0	**8.6**	5.8	1.1	2.4	**4.0**	**3.1**
39	0.6	0.55	**0.7**	0.6	0.8	0.9	**2.5**	1.4	1.9	3.4	**9.8**	5.7	1.3	2.1	**4.4**	**3.0**
40	0.6	0.5	**0.7**	0.7	1.0	0.8	**2.5**	**1.9**	3.3	1.9	**10.0**	5.9	2.0	1.3	**4.4**	**3.3**
41	**0.7**	**0.9**	0.7	0.7	**1.7**	**3.4**	**1.8**	**1.9**	4.0	**8.5**	**7.3**	**7.8**	**2.9**	**4.7**	**3.5**	**3.8**
42	0.5	**0.9**	**0.7**	**0.7**	0.8	**2.3**	**2.5**	**1.9**	1.0	4.8	**10.4**	**6.3**	0.9	**3.1**	**4.6**	**3.3**
43	0.5	0.6	**0.7**	0.7	0.8	1.1	**2.4**	**1.8**	1.1	3.6	**9.4**	**7.8**	1.0	2.2	**4.3**	**3.8**
44	0.6	0.6	**0.7**	**0.7**	0.9	1.0	**2.3**	**2.0**	1.8	3.0	**9.7**	**7.7**	1.3	1.9	**4.3**	**3.7**
45	0.6	**1.2**	**0.8**	**0.8**	0.8	**1.9**	**2.5**	**2.5**	1.8	5.0	**10.4**	**7.4**	1.4	**3.02**	**4.6**	**3.9**

7 Data Availability

Data are available from the corresponding author upon reasonable request.

8 Author Contributions

TSPO: Conceptualization, data curation, formal analysis, investigation, methodology, visualization, writing – original draft preparation (with input from all co-authors). TK: Formal analysis, data curation. BM: Conceptualization, methodology, writing – review and editing. JH: Formal analysis, investigation, writing – review and editing. AA: Conceptualization, writing – review and editing. FC: Conceptualization, supervision, project administration, funding acquisition, writing – review and editing BG: Conceptualization, supervision, project administration, funding acquisition, writing – review and editing.

9 Competing Interests

The authors declare that they have no conflict of interest.

10 Acknowledgements

The authors would like to thank the Autonomous Province of Bolzano - South Tyrol – Department of Innovation, Research, University and Museums for funding the project: Towards an Efficient Design of River Confluences to Manage Intense Sediment Impacts from Tributary Torrents (ECOSED_TT, contract number 24/34). This project and the accompanying funding provided the framework to conduct detailed investigations into mountain-river confluence hydraulics and morphology. Additionally, we acknowledge the funding of the Project Anid/Conicyt Fondecyt Regular Folio 1200091 titled “Unravelling the Dynamics and Impacts of Sediment-Laden Flows in Urban Areas in Southern Chile as a Basis for Innovative Adaptation (sedimpact)” led by the PI Bruno Mazzorana.

11 References

Ancey, C.: Bedload transport: A walk between randomness and determinism. part 1. the state of the art. J. Hydraul. Res., 58(1), 1–17. doi:10.1080/00221686.2019.1702594, 2020a.

Ancey, C.: Bedload transport: A walk between randomness and determinism. part 2. challenges and prospects. J. Hydraul. Res., 58(1), 18–33. doi:10.1080/00221686.2019.1702595, 2020b.

Aufleger, M.: Flussmorphologische Modell. Grundlagen und Anwendungsgrenzen. Berichte des Lehrstuhls und der Versuchsanstalt für Wasserbau und Wasserwirtshaft, TU München. Band Nr. 104: 198-207. TU München, 2006.

Aulitzky, H.: Preliminary two-fold classification of debris torrents, Conference Proceedings of Interpraevent 1980, Bad Ischl, Austria, 8-12 September, Vol. 4, 285-309, 1980, translated from German by G. Eisbacher, Internationale Forschungsgesellschaft, Interpraevent, Klagenfurt.

Aulitzky, H.: The debris flows of Austria, B. Eng. Geol. Environ., 40, 5-13, doi:10.1007/BF02590338, 1989.

Baranovskiy, N. V.: The development of application to software origin pro for informational analysis and forecast of forest fire danger caused by thunderstorm activity, J. Automat. Inf. Sci., 51(4), 12-23, doi:10.1615/jautomatinfscien.v51.i4.20, 2019.

Benda, L., Andras, K., Miller, D., and Bigelow, P.: Confluence effects in rivers: Interactions of basin scale, network geometry, and disturbance regimes, Water Resour. Res., 40(5), 1-15, doi:10.1029/2003wr002583, 2004.

Best, J. L.: Flow Dynamics at River Channel Confluences: Implications for Sediment Transport and Bed Morphology, in: Recent Developments in Fluvial Sedimentology, SEPM Special Publication, edited by: Etheridge, F.G., Flores, R.M. and Harvey, M.D., Society for Sedimentary Geology, Tulsa, OK, 39, 27-35, doi:10.2110/pec.87.39.0027, 1987.

Best, J. L.: Sediment transport and bed morphology at river channel confluences, Sedimentology, 35, 481-498, doi:10.1111/j.1365-3091.1988.tb00999.x, 1988.

724 Biron, P., Roy, A. G., Best, J. L., and Boyer, C. J.: Bed morphology and sedimentology at the confluence
725 of unequal depth channels, Geomorphology, 8(2-3), 115-129. doi:10.1016/0169-555x(93)90032-
726 w, 1993.

727 Biron, P., Roy, A. G., & Best, J. L.: Turbulent flow structure at concordant and discordant open-channel
728 confluences. Exp Fluids, 21(6), 437–446, doi:10.1007/bf00189046, 1996.

729 Blöschl, G., Hall, J., Parajka, J., Perdigão, R. A., Merz, B., Arheimer, B., Aronica, G. T., Bilibashi, A.,
730 Bonacci, O., Borga, M., Čanjevac, I., Castellarin, A., Chirico, G. B., Claps, P., Fiala, K., Frolova, N.,
731 Gorbachova, L., Gül, A., Hannaford, J., … Živković, N.: Changing climate shifts timing of European
732 floods, Science, 357(6351), 588–590, doi:10.1126/science.aan2506, 2017.

733 Blöschl, G., Kiss, A., Viglione, A., Barriendos, M., Böhm, O., Brázdil, R., Coeur, D., Demarée, G., Llasat, M.
734 C., Macdonald, N., Retsö, D., Roald, L., Schmocker-Fackel, P., Amorim, I., Bělínová, M., Benito, G.,
735 Bertolin, C., Camuffo, D., Cornel, D., … Wetter, O.: Current European flood-rich period exceptional
736 compared with past 500 years, Nature, 583(7817), 560–566. doi:10.1038/s41586-020-2478-3, 2020.

737 Boyer, C., Roy, A. G., and Best, J. L.: Dynamics of a river channel confluence with discordant beds: Flow
738 turbulence, bed load sediment transport, and bed morphology, J. Geophys. Res., 111(F4),
739 doi:10.1029/2005jf000458, 2006.

740 Bradbrook, K. F., Biron, P. M., Lane, S. N., Richards, K. S., and Roy, A. G.: Investigation of controls on
741 secondary circulation in a simple confluence geometry using a three-dimensional numerical model,
742 Hydrol. Process., 12(8), 1371-1396. doi:10.1002/(sici)1099-1085(19980630)12:83.0.co;2-c, 1998.

743 Bunte, K., and Abt, S.R.: Sampling surface and subsurface particle size distributions in wadable gravel-
744 and cobble-bed streams for analysis in sediment transport, hydraulics, and streambed monitoring,
745 U.S. Dep. of Agric., For. Serv., Rocky Mt. Res. Stn., Fort Collins, Colorado, USA.Gen. Tech. Rep.
746 RMRS-GTR-74, 428p, doi:10.2737/RMRS-GTR-74, 2001.

747 Chanson, H.: The hydraulics of open channel flow, Butterworth-Heinemann, Oxford, U.K.,
748 doi:10.1016/B978-0-7506-5978-9.X5000-4, 2004.

749 Chow, V.T.: Open Channel Hydraulics, McGraw-Hill, New York, ISBN 9780070859067, 1959.

Darby, S. E., and M. J. Van De Wiel: Models in fluvial geomorphology, in Tools in Fluvial Geomorphology, edited by: G. M. Kondolf and H. Piégay, pp. 503–537, John Wiley, Chichester, U.K., doi:10.1002/9781118648551.ch17, 2003.

Davies, T. R. H., and A. J. Sutherland: Extremal hypotheses for river behaviour, Water Resour. Res., 19, 141– 148, doi:10.1029/WR019i001p00141, 1983.

Delacre, M., Leys, C., Mora, Y., and Lakens, D.: Taking Parametric Assumptions Seriously: Arguments for the Use of Welch's F-test instead of the Classical F-test in One-Way ANOVA, Int. Rev. Soc. Psychol., 32(1), 13, 1-12 doi:10.5334/irsp.19, 2019.

De Serres, B., Roy, A., Biron, P., and Best, J. L.: Three-dimensional flow structure at a river channel confluence with discordant beds, Geomorphology, 26, 313-335, doi:10.1016/S0169-555X(98)00064-6, 1999.

Dunn, O. J.: Multiple comparisons using rank sums, Technometrics, 6(3), 241–252, doi:10.1080/00401706.1964.10490181, 1964.

Embleton-Hamann, C.: Geomorphological Hazards in Austria, in: Geomorphological Hazards of Europe, edited by: Embleton, C., and Embleton-Hamann, C., Elsevier Science Amsterdam, NL, 5, 1-30, doi:10.1016/S0928-2025(97)80002-8, 1997.

Ferguson, R., and Hoey, T.: Effects of Tributaries on Main-Channel Geomorphology, in: River Confluences, Tributaries and the Fluvial Network, edited by: Rice, S.P, Roy, A.G. and Rhoads, B.L., John Wiley & Sons Hoboken, New Jersey, 183-206, doi:10.1002/9780470760383.ch10, 2008.

Gems, B., Sturm, M., Vogl, A., Weber, C., and Aufleger , M.: Analysis of Damage Causing Hazard Processes on a Torrent Fan – Scale Model Tests of the Schnannerbach Torrent Channel and its Entry to the Receiving Water, Conference Proceedings of Interpraevent 2014 in the Pacific Rim, Nara, Japan, 25-28 November 2014, 170-178, 2014.

Gems, B., Kammerlander, J., Aufleger, M., and Moser, M.: Fluviatile Feststoffereignisse, in: ExtremA 2019. Aktueller Wissensstand zu Extremereignissen alpiner Naturgefahren in Österreich, edited by:

Glade, T., Mergili, M., and. Sattler K., Vienna University Press, 287-321, ISBN 9783847110927, 2020.

Guillén-Ludeña, S., Franca, M. J., Cardoso, A. H., and Schleiss, A.: Hydro-morphodynamic evolution in a 90° movable bed discordant confluence with low discharge ratio, Earth Surf. Processes, 40(14), 1927-1938. doi:10.1002/esp.3770, 2015.

Guillén-Ludeña, S., Cheng, Z., Constantinescu, G., and Franca, M. J.: Hydrodynamics of mountain-river confluences and its relationship to sediment transport, J. Geophys. Res.-Earth., 122(4), 901-924. doi:10.1002/2016jf004122, 2017.

Hanus, S., Hrachowitz, M., Zekollari, H., Schoups, G., Vizcaino, M., and Kaitna, R.: Future changes in annual, seasonal and monthly runoff signatures in contrasting Alpine catchments in Austria, Hydrol. Earth Syst. Sc., 25, 3429-3453. doi:10.5194/hess-25-3429-2021, 2021.

Heller, V.: Scale effects in physical hydraulic engineering models. J Hydraul Res, 49(3), 293–306. doi:10.1080/00221686.2011.578914, 2011.

Hübl, J., Ganahl, E., Bacher, M., Chiari, M., Holub, M., Kaitna, R., Prokop, A., Dunwoody, G., Forster, A., Schneiderbauer, S.: Dokumentation der Wildbachereignisse vom 22./23. August 2005 in Tirol, Band 1: Generelle Aufnahme (5W-Standard); IAN Report 109 Band 1, Institut für Alpine Naturgefahren, Universität für Bodenkultur-Wien (unveröffentlicht), 2005.

Hübl, J., and Moser, M.: Risk management in Lattenbach: A case study from Austria, Wit. Trans. Ecol. Envir., 90, 333-342, doi:10.2495/deb060321, 2006.

Hübl J., Eisl J., Tadler R.: Ereignisdokumentation 2012, Jahresrückblick der Ereignisse. IAN Report 150, Band 3, Institut für Alpine Naturgefahren, Universität für Bodenkultur - Wien (unveröffentlicht), 2012.

Kammerlander, J., Gems, B., Sturm, M., and Aufleger, M.: Analysis of Flood Related Processes at Confluences of Steep Tributary Channels and Their Respective Receiving Streams - 2d Numerical Modelling Application, Conference Proceedings of Interpraevent 2016, Lucerne, Switzerland, 30 May-2 June 2016, 319-326, 2016.

801 Keiler, M., Knight, J., and Harrison, S.: Climate change and geomorphological hazards in the Eastern
802 European Alps, Philos. T. R. Soc. A., 368(1919), 2461–2479, doi:10.1098/rsta.2010.0047, 2010.

803 Knight, J., and Harrison, S.: Sediments and future climate, Nat. Geosci., 2(4), 230–230, doi:
804 10.1038/ngeo491, 2009.

805 Lane, E.W.: The importance of fluvial morphology in hydraulic engineering. J. Hydraul. ENG-ASCE, 81, 1–
806 17, 1955.

807 Leite Ribeiro, M., Blanckaert, K., Roy, A. G., and Schleiss, A. J.: Hydromorphological implications of local
808 tributary widening for river rehabilitation, Water. Resour. Res., 48(10), 201-217,
809 doi:10.1029/2011wr011296, 2012a.

810 Leite Ribeiro, M., Blanckaert, K., Roy, A. G., and Schleiss, A. J.: Flow and sediment dynamics in channel
811 confluences J. Geophys. Res-Earth., 117, F01035-, doi:10.1029/2011jf002171, 2012b.

812 Liu, T., Fan, B., and Lu, J.: Sediment-flow interactions at channel confluences: A flume study, Adv. Mech.
813 Eng., 7(6), 1-9, doi:10.1177/1687814015590525, 2015.

814 Löschner, L., Herrnegger, M., Apperl, B., Senoner, T., Seher, W., and Nachtnebel, H.P. : Flood risk, climate
815 change and settlement development: a micro-scale assessment of Austrian municipalities. Reg.
816 Environ. Change. 17, 311–322, doi:10.1007/s10113-016-1009-0, 2017.

817 Massey, F. J.: The Kolmogorov-Smirnov test for goodness of fit, J. Am. Stat. Assoc., 46(253), 68-78,
818 doi:10.1080/01621459.1951.10500769, 1951.

819 Maxwell, S. E., and Delaney, H. D.: Designing experiments and analyzing data (2nd ed.), Routledge, New
820 York, doi:10.4324/9781410609243, 2004.

821 McKnight, P.E. and Najab, J.: Mann-Whitney U Test. in: The Corsini Encyclopedia of Psychology 1-1, John
822 Wiley & Sons, Hoboken, New Jersey, doi:10.1002/9780470479216.corpsy0524, 2010.

823 Meunier, M.: Éléments d'hydraulique Torrentielle, Cemagref, France, EAN13 9782759212088, 1991.

824 Miller, J.P.: High mountain streams: effects of geology on channel characteristics and bed material. Mem.
825 State Bureau of Mines and Mineral Resources, New Mexico Institute of Mining & Technology,
826 Socorro, New Mexico , 4, 1958.

827 Moder, K.: Alternatives to F-test in one-way ANOVA in case of heterogeneity of variances (a simulation
828 study). Psychological Test and Assessment Modeling, 52(4), 343-353, ISSN 2190-0493, 2010.

829 Mosley, M. P.: An experimental study of channel confluences, J. Geol., 84(5), 535-562,
830 doi:10.1086/628230, 1976.

831 Mueller, E. R., and Pitlick, J.: Morphologically based model of bed load transport capacity in a headwater
832 stream, J. Geophys. Res., 110(F2), doi:10.1029/2003jf000117, 2005.

833 Oliveto, G., Hager, W.H.: Further results to time dependent local scour at bridge elements. J. Hydraulic
834 Eng.131(2), 97–105, doi:10.1061/(ASCE)0733-9429(2005)131:2(97), 2005.

835 Penna, N.; De Marchis, M.; Canelas, O.B.; Napoli, E.; Cardoso, A.H.; Gaudio, R.: Effect of the Junction
836 Angle on Turbulent Flow at a Hydraulic Confluence. Water, 10, 469, doi:10.3390/w10040469, 2018.

837 Prenner, D., Hrachowitz, M., and Kaitna, R.: Trigger characteristics of torrential flows from high to low alpine
838 regions, Austria, Sci. Total. Environ., 658, 958-972, doi:10.1016/j.scitotenv.2018.12.206, 2018.

839 Rhoads, B. and Kenworthy, S.: Flow structure at an asymmetrical confluence. Geomorphology, 11, 273-
840 293, doi:10.1016/0169-555X(94)00069-4, 1995.

841 Rice, S.: Which tributaries disrupt downstream fining along gravel-bed rivers? Geomorphology, 22(1), 39 –
842 56, doi:10.1016/s0169-555x(97)00052-4, 1998.

843 Roca, M., Martín-Vide, J.P., and Martin-Moreta, P.: Modelling a torrential event in a river confluence, J.
844 Hydrol., 364, 207-215, doi:10.1016/j.jhydrol.2008.10.020, 2009.

Rom, J., Haas, F., Hofmeister, F., Fleischer, F., Altmann, M., Pfeiffer, M., Heckmann, T., and Becht, M.: Analysing the large-scale debris flow event in July 2022 in Horlachtal, Austria, using remote sensing and measurement data, Geosci. J., 13(4), 100, doi:10.3390/geosciences13040100, 2023.

Roy, A., and Bergeron, N.: Flow and particle paths at a natural river confluence with coarse bed material, Geomorphology, 3(2), 99-112, https://doi: 10.1016/0169-555x(90)90039-s, 1990.

Rudolf-Miklau, F., Suda, J.: Design Criteria for Torrential Barriers, In: Dating Torrential Processes on Fans and Cones. Advances in Global Change Resource, vol 47, edited by: Schneuwly-Bollschweiler, M., Stoffel, M., Rudolf-Miklau, F., Springer, Dordrecht, doi:10.1007/978-94-007-4336-6_26, 2013.

Ruxton, G. D., and Beauchamp, G.: Time for some a priori thinking about post hoc testing, Behav. Ecol., 19/3, 690-693, doi:10.1093/beheco/arn020, 2008.

Sawyer, S.: Analysis of Variance: The Fundamental Concepts, J. Man. Manip. Ther., 17, 27E-38E, doi:10.1179/jmt.2009.17.2.27E, 2009.

Steinskog, D. J., Tjøstheim, D. B., and Kvamstø, N. G.: A cautionary note on the use of the Kolmogorov–Simonov test for normality, Mon. Weather. Rev., 135(3), 1151-1157, doi:10.1175/mwr3326.1, 2007.

Stevenson, K. J.: Review of OriginPro 8.5, J. Am. Chem. Soc., 133(14), 5621-5621, doi:10.1021/ja202216h, 2011.

Stoffel, M.: Magnitude–frequency relationships of debris flows - a case study based on field surveys and tree-ring records, Geomorphology, 116(1–2), 67–76, doi:10.1016/j.geomorph.2009.10.009, 2010.

Stoffel, M., and Huggel, C: Effects of climate change on mass movements in mountain environments, Prog Phys. Geog., 36(3), 421–439, doi:10.1177/0309133312441010, 2012.

St. Pierre Ostrander, T., Holzner, J., Mazzorana, B., Gorfer, M., Andreoli, A., Comiti, F., and Gems, B.: Confluence morphodynamics in mountain rivers in response to intense tributary bedload input, Earth Surf. Processes, 1-22, doi:10.1002/esp.5613, 2023.

868 Sturm, M., Gems, B., Keller, F., Mazzorana, B., Fuchs, S., Papathoma-Köhle, M. and Aufleger, M.:
869 Experimental analyses of impact forces on buildings exposed to fluvial hazards, J. Hydrol., 565, 1-
870 13, doi:10.1016/j.jhydrol.2018.07.070, 2018.

871 Trevisani, S., Cavalli, M., and Marchi, L.: Reading the bed morphology of a mountain stream: A
872 geomorphometric study on high-resolution topographic data, Hydrol. Earth Syst. Sc., 14(2), 393-405,
873 doi:10.5194/hess-14-393-2010, 2010.

874 Wang, X. K., Wang, X., Lu, W., and Liu, T.: Experimental study on flow behavior at open channel
875 confluences, Front. Struct. Civ. Eng., 1, 211-216, doi:10.1007/s11709-007-0025-z, 2007.

876 Welch, B. L.: The generalization of 'student's' problem when several different population variances are
877 involved, Biometrika, 34 (1–2), 28–35 doi:10.1093/biomet/34.1-2.28, 1947.

878 White, W. R., R. Bettess, and Paris, E.: Analytical approach to river regime, J. Hydraul. Div. Am. Soc. Civ.
879 Eng., 108, 1179– 1193, doi:10.1061/JYCEAJ.0005914, 1982.

880 Williams, G. P.: Flume width and water depth effects in sediment-transport experiments - Sediment transport
881 in alluvial channels, USGS Professional Paper, doi:10.3133/pp562h, 1970.

882 Witte, R. S., & Witte, J. S.: Statistics 11th Edition. Wiley and Sons, Hoboken, New Jersey, ISBN 1119386055,
883 2017.

884 Wohl, E. E..: Mountain rivers revisited. American Geophysical Union/Geopress, Washington, D.C., ISBN
885 9780875903231, 2010.

886 Yang, C. T.: Minimum unit stream power and fluvial hydraulics, J. Hydraul. Div. Am. Soc. Civ. Eng., 102,
887 919– 934, doi:10.1061/JYCEAJ.0004589, 1976.

888 Yang, C. T., and C. C. S. Song: Theory of minimum rate of energy dissipation, J. Hydraul. Div. Am. Soc.
889 Civ. Eng., 105, 769–784, doi:10.1029/WR017i004p01014, 1979.

890 Young, W. J., & Warburton, J.: Principles and practice of hydraulic modelling of braided gravel-bed rivers.
891 J. Hydrol. (N.Z.), 35(2), 175–198, 1996.

892 Zarn, B.: Lokale Gerinneaufweitung: Eine Massnahmezur Sohlenstabilisierung der Emme bei Utzenstorf
893 (Localriver expansion: A measure to stabilize the bed of Emme River at Utzendorf). VAW Mitteilung
894 118. D. Vischer ed.ETH Zurich, Zürich [in German], 1992.